Internal Ballistics Simulation Study of Propellant Geometry for Optimal Combustion and Packing Density

AA Alotaibi

0000-0002-1898-4226

Dissertation accepted in partial fulfilment of the requirements for the degree Master of Science in Mechanical Engineering at the Potchefstroom Campus of the North West University

Supervisor: Prof. Willem den Heijer

Co-Supervisor: Mr. Victor Schabort

Graduation: June 2021

Student number: 27360164

DEDICATION AND ACKNOWLEDGEMENTS

I dedicate this dissertation to my beloved parents, who have been my source of inspiration and strength throughout my life's journey. They dedicated their lives to support and inspire me. My love and gratitude to them can never be quantified. I also dedicate this research to my brother Talaq who encouraged me, as well as all my brothers and sisters, who shared their advice and gave their support throughout this journey.

Finally, I dedicate this dissertation to my co-supervisor, who encouraged and supported me throughout my research.

The successful completion of my research required guidance and assistance from several people, to whom I am extremely thankful for their contributions. I wish to acknowledge the following people with love and respect:

- Professor Willem den Heijer, who effectively guided me throughout my study as my supervisor.
- Mr. Victor Schabort, as my co-supervisor, who encouraged me and guided me in understanding the critical elements of the research. The completion of the study would not have been possible without his guidance.
- My colleagues in Military Industries Corporation (MIC) for their support, assistance, and cooperation when I consulted with them. They have helped and inspired me in every step of this research and acted as a constant support structure for me throughout the study. Moreover, I would also like to thank all the members of MIC for providing me with the desired scope and opportunity to develop my career by expanding my knowledge within this research field.
- The research and development team for their valuable support at Rheinmetall Denel Munition (RDM), which provided me with the platform to enhance my skills and knowledge within this field of research.

ABSTRACT

Keyword(s): propellant grains, muzzle velocity, projectile performance, maximum pressure, packing density, propellant burnout.

A conventional bullet or projectile, driven by the rapidly expanding gas formed by the combustion of the propellant charge, accelerates in the barrel and reaches a certain muzzle velocity, spin, and propulsion energy. The geometric characteristics of the propellant grains are one of the primary factors which affect the performance of a projectile and its maximum achievable range. The geometric shape of the propellant grains is crucial to ensure simultaneous burnout of the entire charge before the projectile is discharged from the barrel to prevent unburnt propellant from forming residue inside the gun chamber. The geometrical shape of the propellant grains plays a significant role in the performance of a gun system. This also affects the packing density of the charge. In this research, a proposed propellant grain geometry for a 155 mm artillery gun system was investigated and compared to the rosette grain as a reference propellant grain. This was done to investigate and determine the effects of propellant geometry on the grain size, the packing density, the maximum pressure, and the muzzle velocity.

the proposed propellant grain is outperformed by the rosette grain in term of performance. However, the developed propellant grain achieves higher packing density than the rosette grain. This research establishes a framework that to be used to develop any new propellant grain.

TABLE OF CONTENTS

LIST OF TABLES

LIST OF FIGURES

ABBREVIATIONS AND TERMS

DBP	Double-base propellant
IB	Internal ballistic
IB0D	Internal Ballistic 0-Dimensional Model
IB1D	Internal Ballistic 1-Dimensional Model
IB2D	Internal Ballistic 2-Dimensional Model
LPM	Lumped parameter model
Max P	Maximum pressure
MCS	modular charge system
MIC	Military Industries Corporation
MV	muzzle velocity
NATO	North Atlantic Treaty Organization
NQ	Nitrocellulose
Perf	Perforation
PTV	Pressure Travel Velocity
RDM	Rheinmetall Denel Munition
SBP	Single base propellant
STANAG	Standardization Agreement
TBP	Triple base propellant

NOMENCLATURE

A_x/A_0	Initial grain area
$\overline{C_p}$	Specific heat at constant pressure of propellant gas
T_{0_I}	Adiabatic flame temperature of the igniter
T_{0_i}	Adiabatic flame temperature of i^{th} propellant
T_{0_w}	Initial temperature of chamber wall
$\dot{\boldsymbol{v}}_{\boldsymbol{p}}$	Acceleration of projectile
h_0	Free convective heat transfer coefficient for air in the gun tube
A_{br}	Area of breech face
A_w	Chamber wall area plus the area of gun tube wall exposed to the propellant gases
A_w	Chamber wall area plus area of gun tube wall exposed to propellant gases
C_I	Initial mass of igniter
C_T	Total mass of propellants and igniter
C_{pw}	Heat capacity of steel of chamber wall
D_b	Diameter of bore
D_w	Chamber wall thickness heated
E_h	Energy loss due to heat transfer to the chamber and barrel walls
E_{br}	Energy loss due to friction and engraving of rotating band
E_d	Energy loss due to air resistance (drag)
E_p	Energy loss due to propellant gas and unburned propellant motion
E_{pr}	Energy loss due to projectile rotation
E_{pt}	Energy consumed due to projectile translation
E_r	Energy loss due to recoil
F_I	Force per unit mass of igniter propellant
F_i'	Adjusted force per unit mass of i^{th} propellant
P'_R	Adjusted resistive pressure of the bore due to friction and engraving
P_0	Breech pressure
P_R	Resistive pressure of the bore due to friction and engraving
P_a	Pressure in the ambient air

P_b	Pressure on base of projectile
P_g	Pressure of gas or air ahead of projectile
T_W	Twist of rifling
T_c	Temperature of the chamber wall
α	Burning rate exponent
$\bar{P}$	Surrounding pressure
V_{P_i}	Volume of parasitics associated with i^{th} propellant
V_0	Volume of empty gun chamber
V_c	Volume behind projectile
$\frac{dZ}{dt}$	Mass fraction burning rate of the propellant grain
b_I	Covolume of igniter
b_i	Covolume of i^{th} propellant
f_r	Down-tube resistance factor
m_p	Mass of projectile
m_{rp}	Mass of the recoiling parts
$\bar{v}$	Mean gas velocity
v_p	Velocity of projectile
v_{rp}	Velocity of the gun recoil
x_{rp}	Displacement of the gun recoiling
$\boldsymbol{C_{gas}}$	Mass of propellant gas
$\boldsymbol{C_{solid}}$	Mass of solid propellant grains
$\boldsymbol{V_g}$	Initial volume of the propellant grain
α_a	Ratio of specific heats for air
γ_I	Ratio of specific heats for igniter
γ_i	Ratio of specific heats for i^{th} propellant
$\bar{\rho}$	Mean gas density
ρ_i	Density of i^{th} propellant.
ρ_w	Density of chamber wall steel
h	Heat transfer coefficient of Nordheim, Soodak, and Nordheim
A	Area of base of projectile including appropriate portion of rotating band
AGP	Surface Area of the grain with all perforations
AP	Surface Area of the perforations

$AP1$	Perforation surface area 1
$AP2$	Perforation surface area 2
C	Initial total mass of propellant
D	Grain diameter
DG	Diameter of groove
DL	Diameter of lands
$DP1$	Perforation diameter 1
$DP2$	Perforation diameter 2
Dp	Surface area of the grain without perforations
GLR	Groove-to-land width ratio
ID	Inner diameter of the grain
IDP	The inner diameter of the perforation
IP	Web thickness
IP	Web thickness
L	Grain length
M	Mach number of the projectile with respect to the air
NG	Number of the side grain
NS	The number of the side perforations
OD	Outer diameter
ODP	The outer diameter of the perforation
RG	The radius of the side grain
Sr	Grain surface area
SG	Length of the side grain
SP	Length of the side perforation
V	Grain volume
Z	The fraction of mass burned of the propellant equation
n	Number of propellants
p	Number of perforations
β	Burning rate coefficient
t	Time
$t1$	Normal dimension
$t3$	Smallest dimension
x	Travel of the projectile
ε	Ballistic mass ratio
θ	The opening angle in degrees

λ Nordheim friction factor

Chapter 1: INTRODUCTION

1.1 Background

A gun system is primarily designed to pneumatically propel a projectile. Consequently, a gun shares similarities with a single stroke internal combustion engine, but with only one stroke fired. This concept is shown in Figure 1. In this figure, the projectile is analogous to the piston, and the combusting air-fuel mixture, which drives the projectile, represents the combustion gases resulting from the ignited and combusting propellant. (Carlucci & Jacobson, 2018)

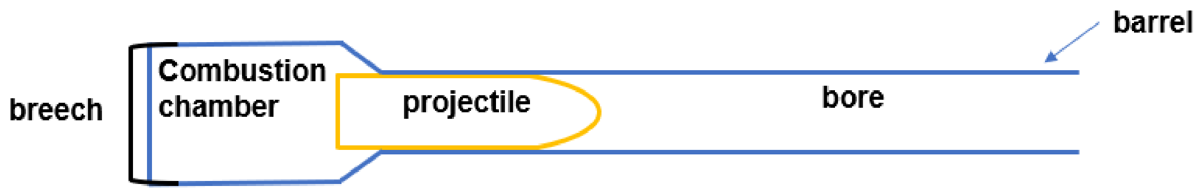

Figure 1: A gun system works as a single stroke internal combustion engine

Gun propellant is a strong and metastable energetic material with the ability to produce hot gases that contain a large amount of energy. A propellant is smokeless, stable, powerful. They are produced in the form of loose grains, which are usually stored in metallic or combustible cases (Kent, 2003).

The term 'gun propellant' is a generic term used for propellant chemicals needed for propelling projectiles from guns and other firearms. Gun propellants are available in certain varieties based on their chemical makeup and the intended application. They are categorised as either single-base propellant (SBP), double-base propellant (DBP), or triple-base propellant (TBP).

single-base propellant contains primarily nitrocellulose (NC) as its primary explosive ingredient. NC is composed of nitrated cotton fibres (cellulose). Additives and stabilisers are used to regulate the chemical stability and improve the properties. The ignition temperature of NC is approximately 315 ºC, and its flame temperature ranges between 2230 °C and 2730 ºC. It is classified as a cool-burning propellant due to its relatively low burning temperature. The energy content of SBP reaches up to 1050 J/g, which is the lowest among the various propellant types (Kubota, 2007).

Double-base propellant is primarily composed of NC with nitro-glycerine or other liquid organic nitrate explosives added. The presence of nitro-glycerine elevates the energy content, the flame temperature, and reduces the ignition temperature. The ignition temperature of DBP is approximately 145 ºC, and its flame temperature ranges between 2330 °C and 3330 ºC. DBP has an energy content of approximately 1170 J/g, making it the most sensitive and powerful of the various propellant types (Kubota, 2007).

Triple-base propellant incorporates an additional energetic component in conjunction with NC and nitro-glycerine, namely nitro-guanidine, or another liquid organic nitrate explosive. TBP has a moderately higher energy content at a relatively lower flame temperature. A typical TBP contains energy equal to approximately 1100 J/g (Kubota, 2007).

The gas generated from combusting propellant grains drives the ballistic systems. Ballisticians can influence the entire ballistic system to meet their design requirements. This is achieved by manipulating the rate of gas produced by the propellant grains, which includes manipulation of the chemical composition of the propellant. The rate of gas production from various propellants can further be controlled by means of the exposed surface of the grain. The generation of propellant gas is dependent on the surface area of the grain. This makes the geometric shape of the propellant grain extremely important in terms of its impact on the IB cycle. Propellant grain geometry is consequently a critical factor that enables the optimisation of the performance of the ballistic system. (Carlucci D. J., 2007)

There are numerous propellant grains available that have varying shapes to deliver specific gas production profiles. Propellant grains are categorised as digressive-, neutral-, and progressive burning grains (Carlucci D. J., 2007).

A digressive burning grain will reduce its total surface area over time as it burns. As the total surface area reduces over time, there will be a corresponding reduction in gas production over time. The initial phase of burning for digressive grains represents the maximum rate of gas generation. Digressive grains consequently increase the gun chamber pressure more rapidly during the initial portion of burning. Digressive grains accelerate the projectile faster in the initial portion of the barrel. This allows the projectile to reach its maximum velocity at the initial stage of the barrel (Carlucci D. J., 2007).

The total surface area of a neutral burning grain is designed to remain constant over time once it starts to combust. This means that gas generation almost remain constant over time until the grain is completely combusted, if it is assumed the surrounding pressure is constant. Figure 2 provides an example of a neutral burning grain (perforated cylindrical grain). The perforation diameter of a neutral burning grain expands outwards, thus increasing the surface area, while the outer diameter is reduced accordingly, thus decreasing the surface area, as it burns. This increase in the surface area of the perforation and the decrease in the surface area of the outside surface effectively compensate for each other, keeping the entire exposed surface area unchanged (Carlucci D. J., 2007). This mechanism keeps the rate of gas generation constant from ignition to the point of complete combustion in neutral grains.

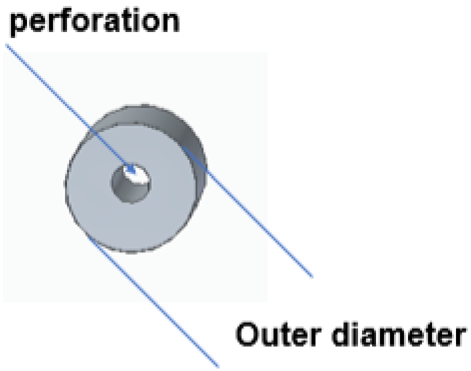

Figure 2: Single perforation grain

Finally, progressive burning grains have a geometrical design which enables the total surface area to increase over time as it burns. The rate of gas generation consequently increases over time to a point whereafter it rapidly diminishes. Figure 3 shows an example of a progressive burning grain (multi-perforated cylindrical grain). As it burns, the seven perforations grow larger in diameter with a corresponding increase in surface area. The outer diameter reduces with a corresponding reduction in the surface area. This mechanism results in the total surface area effectively increasing over time (Carlucci D. J., 2007).

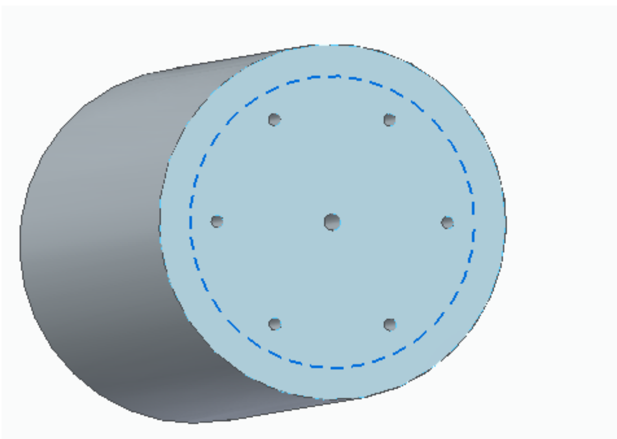

Figure 3: Seven perforation grain

Progressive grains increase the chamber pressure more slowly than the other grains because the generated gas at the initial stage of burning is relatively less and it moves the projectile allowing it to increase the chamber volume due to projectile displacement. As a result, the maximum rate of gas generation in progressive burning grains is experienced at the final phase of burning (Command., 2019). The progressive propellant is widely used in large calibre systems.

1.2 Internal ballistic cycle

The IB cycle examines the internal performance of a gun system. The IB cycle involves the ignition of the propellant, the motion of the projectile through the gun system, as well as the motion of the gun from the point of the combustion of the propellant to the point in time when the projectile leaves the muzzle of the gun system. While the IB cycle appears to be the same in most gun systems, some details differ from one system to another.

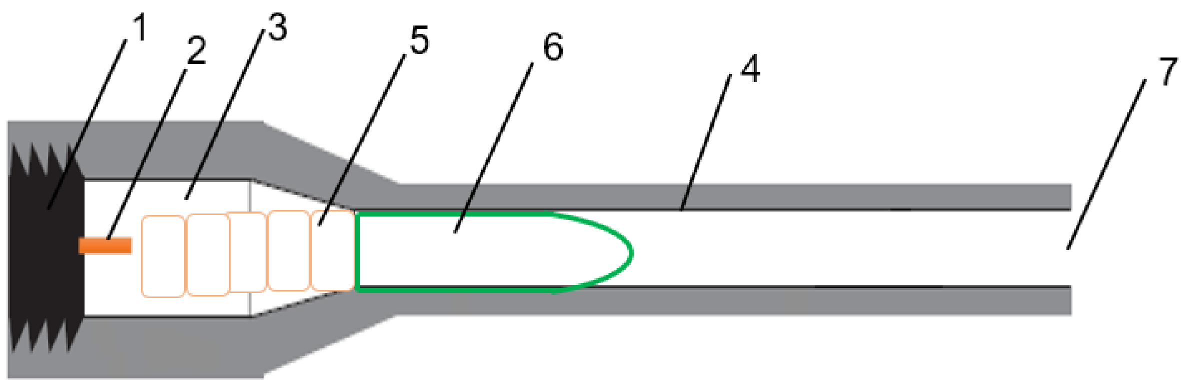

Figure 4: Schematic diagram of a generic internal ballistic system

A general IB system, as illustrated in Figure 4, includes the breech (1), the igniter (2), the combustion chamber (3), the barrel (4), the propellant (5), the projectile (6) and the muzzle (7).

The chronological steps of a generic ballistic system begin when the igniter device explodes. Hot gases and burning particles are then spread through the solid propellant grains as illustrated in Figure 5. The grains of the solid propellant are ignited and start to burn. As the propellant burn, it releases hot gas that contains large quantities of energy.

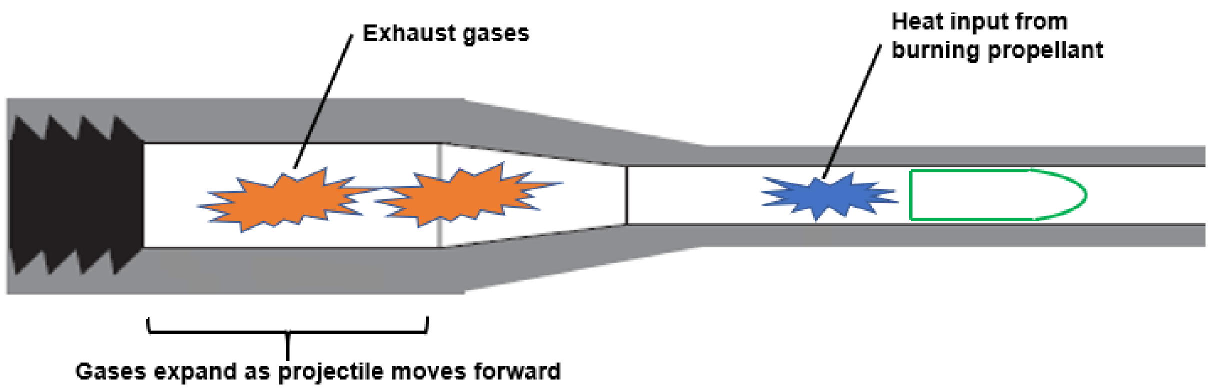

Figure 5: Illustration of the IB cycle initiation

The combustion of the solid propellant grains and their conversion to hot gas will result in incremental increases in the pressure and temperature inside the gun chamber. The increasing pressure inside the gun chamber forces the solid propellant grains to burn at an accelerated rate, which triggers a rapid increase in the pressure in the gun chamber. The high gas pressure inside the gun chamber exerts a force on the base of the projectile, the chamber sidewalls and the breechblock. When a sufficient pressure level is exerted on the base of the projectile, the projectile starts to move and is propelled through the gun barrel. As the projectile accelerates within the barrel, the effective volume of the gun chamber increases since it now includes the increasing volume of the gun barrel as well. The pressure inside the gun chamber starts to decrease as the projectile continues to increase its velocity due to the gas mass flow produced by the burning solid propellant grains. At a certain point the solid propellant grains are fully burnt out whilst the expanding gas mass is still sufficient to propel the projectile even further within the gun barrel. The projectile then leaves the gun muzzle with a high muzzle velocity. The projectile is followed by a blast discharge from the barrel which is caused by a significant pressure wave in Figure 6.

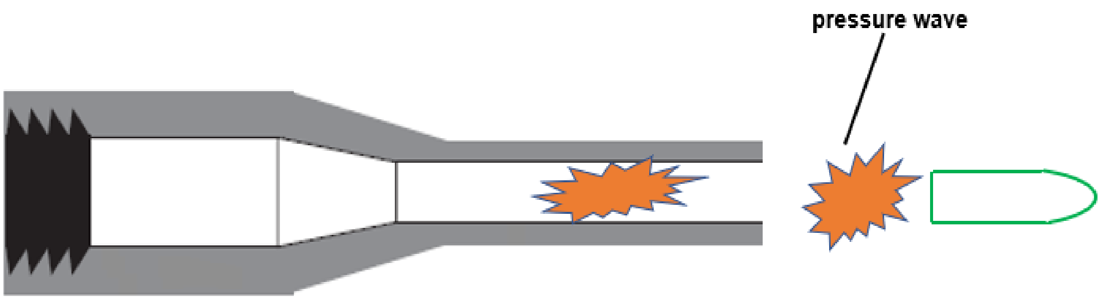

Figure 6: Gas discharge from the muzzle (Dyckmans, 2015)

The duration of an IB cycle only lasts for a few milliseconds for small- and medium calibre gun systems. It can however take up to 15 milliseconds for a large calibre system. The pressure profile and the projectile velocity profile during the IB cycle is illustrated in Figure 7 (Dyckmans, 2015).

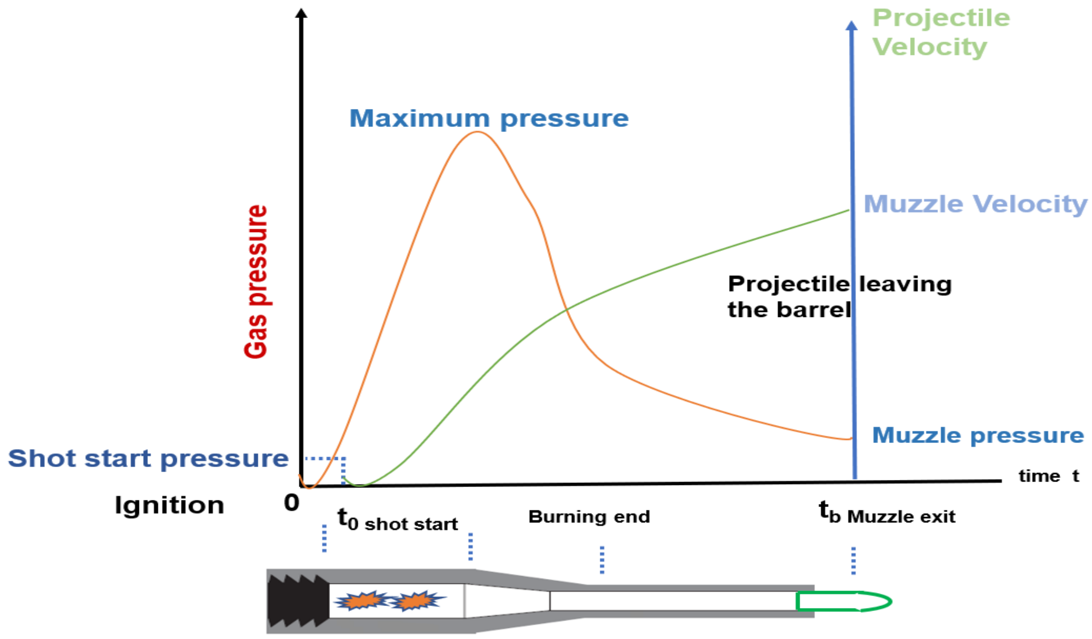

Figure 7: Chamber pressure vs projectile velocity along with the time and projectile displacement (Dyckmans, 2015)

As the projectile travels within the barrel, a graph is drawn where the x-axis represents the barrel length. The resulting curve is known as the PTV (Pressure, Travel, and Velocity) curve and is considered as the basic tool for internal ballistic system analysis. The PTV diagram trend and its specifications are mainly related to the gun system and the properties of the propellant such as grain size and its rate of combustion (Dyckmans, 2015).

1.3 Problem statement

In large calibre gun system, the multi-perforated grain is the most common used grain type of progressive burning propellants. However, United States patent No. US5821449A have found that multi-perforated grains produce residues, which are unburned propellant during combustion. These residues are also known as slivers. They reduce the efficiency of the gun system and reduce its lifespan (United States Patent No. US5821449A, 1995). Ballisticians concluded that once the multi-perforated grain ignites, the perforations, which are holes in the surface of the propellant grain, start to enlarge. When the seven perforations overlap, the propellant grain stops burning, which leaves unburned pieces of propellant in the system. Figure 8 demonstrates the burning stages of the multi-perforated grain.

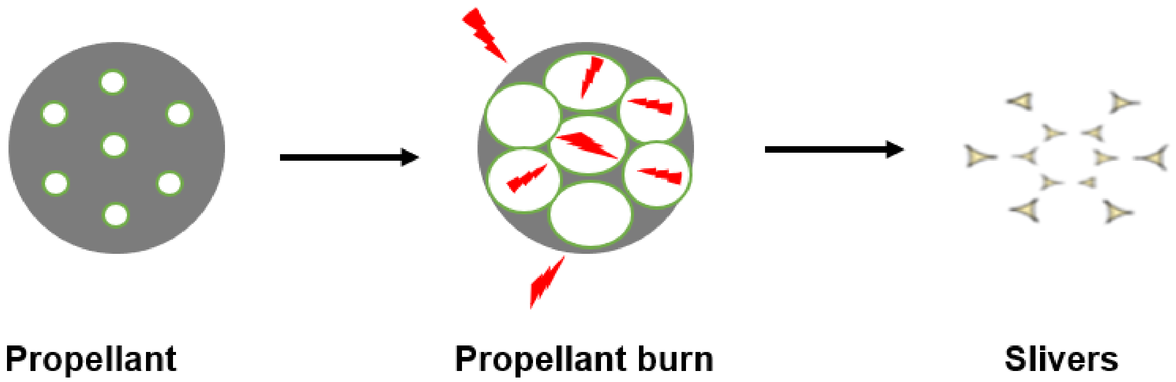

Figure 8: Formation of slivers

Investigations into multi-perforated propellant grain geometries have shown that slivers are generated that leads to significant residue build-up inside the gun system. The geometry was modified to reduce the outer slivers to address this effect. This resulted in the rosette grain as shown in Figure 9. The rosette grain design does not eliminate the inner slivers and the challenge of slivers and residue build-up remains to some extent. Sliver residue is a key cause of operational- and safety problems during firing (RDM, 2018). The presence of sliver residue implies that propellant grains have not fully burned and the performance of the gun system is reduce.

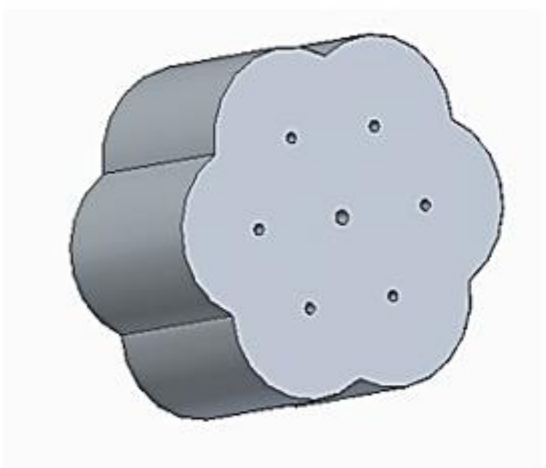

Figure 9: Rosette propellant grain shape

Nowadays, the rosette grain is the most utilised configuration of propellant grain for large calibre systems. It is claimed by the scientific community that specialises in propellants that rosette grain is the optimal configuration for large calibre weapons where it offers better performance. However, the rosette grain has inherent disadvantages , which is the inner sliver formation and sub-optimal packing density. According to Schabort, inner sliver formation causes residues inside the gun system during serial firing (Schabort, 2016).

Propellant grains with minimal sliver formation perform much better than propellant grains that exhibit sliver formation. Therefore, it is crucial to investigate and design an optimal shape for a propellant grain that would enable optimal combustion, which might improve the gun system performance.

1.4 Aim of this research

This research aims to investigate and design a new propellant grain geometry that would improve the ballistics of large calibre gun systems. However, the slivering computation will not be part of the proposed burning simulation. Thus, during the slivering computation, it is assumed that there is no sliver formation during combustion. The proposed propellant grain geometry should also achieve better packing density while retaining good propellant ignition to comply with the required characteristics of the PTV diagram and optimise the area under the curve.

1.5 Method of investigation

The following investigation methods will be followed during this research:

1. Research and investigate existing propellant geometries.

2. Propose a new propellant grain geometry that addresses the disadvantages of the existing grain geometries in terms of sliver formation and packing density.

3. Examine the proposed geometry using the Solid Edge software. The Solid Edge software has several functionalities that allow for the visualisation of the combustion behaviour of the propellant grain. As a result, the proposed propellant geometry can be simulated for optimal combustion and minimised sliver formation.

4. After examining the proposed propellant geometry, a form function equation shall be developed according to the STANAG 4367 specification. Form function equations are

analytical equations that calculate the surface area and volume of the propellant grain in order to determine the gas delivery profile.

5. Verify the result of the form function equation against the result from the Solid Edge software.
6. Build an internal ballistic simulation model and verify it against the existing RDM model.
7. Conduct an internal ballistic analysis of the proposed grain geometry to find the optimal dimensions of the proposed grain and the optimal charge mass.
8. Compare the proposed grain against the rosette grain, in terms of the performance and packing density of the 155 mm artillery system.

1.6 Limitations

1. This research is based only on theory.
2. There is no validation for the proposed design of the propellant grain.
3. The slivering analysis of the proposed design of the propellant grain is not part of this research.

1.7 Dissertation outline

This section provides a brief overview of the dissertation.

Chapter 1

Chapter 1 provides a basic overview of the gun system. It breaks down the system into the major components, i.e., the chamber that contains the propellant, the barrel that is meant to increase the bullet's acceleration, the muzzle, and the breech. The chapter also provides the aim of the research paper.

Chapter 2

This chapter provides the background literature that has been used. It will also explore some of the areas that this research did not cover. Finally, it looks into the events that occur during a gun's combustion.

Chapter 3

This chapter describes energy model, motion model, state model, combustion model and the pressure gradient model all these processes in detail, together with the equations and calculations involved. The final part of the chapter looks at the verification process for the IB0D models, which must comply with STANAG 4367 and be verified against the RDM simulation program.

Chapter 4

This chapter focuses on the proposed geometric design of the propellant grain. The design process incorporates the use of parametric modelling, including MATLAB and IB0D, which involves the calculation of various ballistic properties.

Chapter 5

Various parameters are evaluated to determine the muzzle velocity and the maximum pressure. This includes the analysis of charts and graphs as well as determining the compatibility of the design. It also outlines the pros and cons of the proposed grain.

Chapter 6

Summarizes the results, findings, and conclusions in conjunction with suggestions for future research.

1.8 Summary

Chapter 1 provides background on gun systems and their various components. From the analysis, it is evident that the gun system has four major parts: the combustion chamber that contains the propellant, the barrel where the projectile is accelerated, the muzzle where the projectile leaves the barrel and the breech, which is the rear side of the gun.

The research problem, research aim, and objective of the research are stated. The project aims to design new propellant grain geometry to achieve the optimum charge packing density while retaining propellant ignition, with minimised sliver formation.

Chapter 2: LITERATURE REVIEW

2.1 Introduction

In this chapter, the burning behaviour of the propellant grains will be described. In addition, the slivering due to propellant combustion will be described. Also, in this chapter, the web of the propellant and its effects on the gun system performance will be described. The packing density also will be described.

2.2 Burning configuration of the propellant

The chemical and physical properties need to be established in order to model a propellant grain. The grain geometry is one of the critical parameters of the propellant (Miner, 2013). Solid propellants can have various grain geometries, which include flake-, perforated tubular-, ball- (sphere) and solid tabular geometries (Miner, 2013). Miner argues that similar propellants must burn in different ways due to differences in size and shape. The burning area is characterised by three main types consisting of progressive-, neutral- or digressive burning. The burning area type gives a description of the extent of the surface area of the propellant grain that is exposed while it burns. A progressive burn type has a surface area which enlarges throughout the combustion process. A neutral burn type has the same surface area throughout the combustion process. A digressive burning rate has a continuously decreasing combustion surface area as it undergoes combustion.

Figure 10 indicates the different propellant geometries, where A is digressive burning, B is neutral burning, and C is progressive burning (Zeller, 1993).

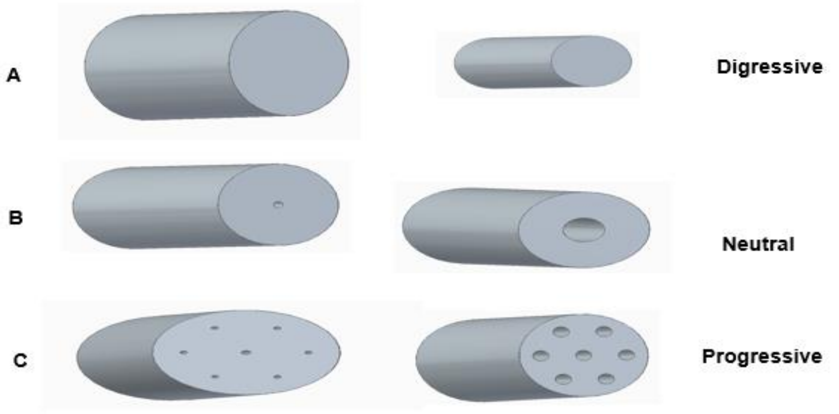

Figure 10: Different triple-base propellant geometries.

Figure 11 indicates the different burning rates for grain geometries. There is an extensive range of propellants; it is therefore vital to choose the right grain propellant for the appropriate ballistic system or design (Shekhar, 2015).

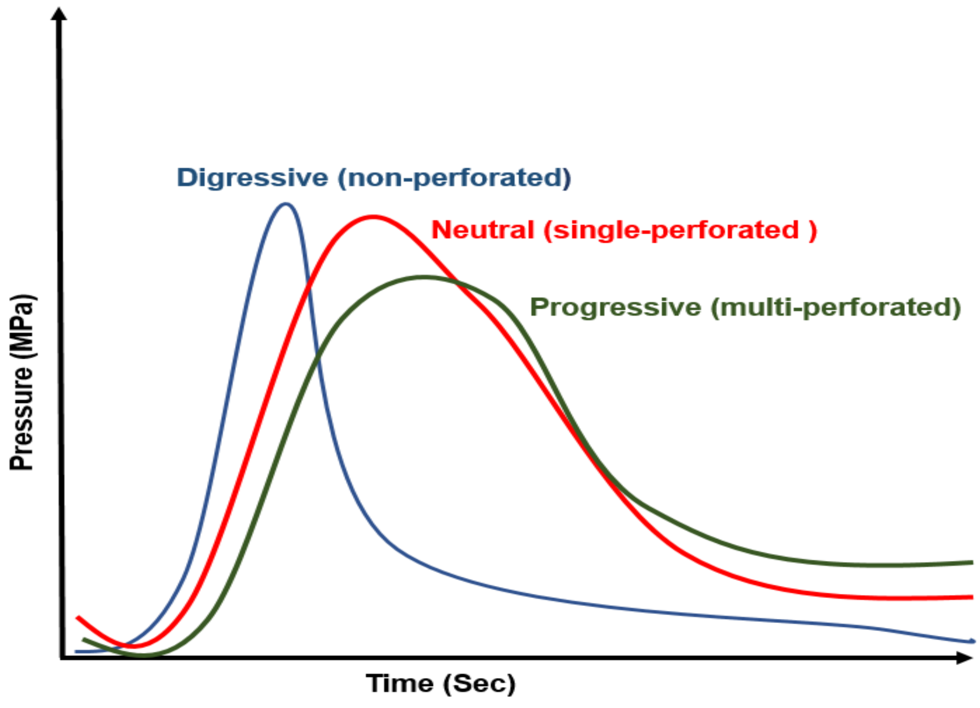

Figure 11: pressure-time curves for different propellant geometries in gun system

2.3 Propellant burning rate profile

The burning surface of the propellant grain is usually oriented in a direction normal to the physical surface of the grain. The burning rate can be described as the linear regression rate of the edge of the flame, measured at a specific distance and time on the burning surface of the propellant.

Factors that affect the burning rate of the propellant are the initial temperature, and the pressure inside the burning chamber. Considering a grain of known composition, the relationship of the burning rate to the propellant and all the parameters that govern the process is called the "burning rate" of the propellant. The following empirical equation is commonly used to express the burning rate of a propellant (National Aeronautics, 1972):

$$r = \beta(\bar{P})^{\alpha}$$

Equation 2-1

Where:

β	Burning rate coefficient.
α	Burning rate exponent.
$\bar{P}$	Surrounding pressure.

Propellant charge ballistics is a function of the rate at which gas is generated as the propellant burns. Ballistic properties are consequently dependent on the energy content and energy release of the propellant (Atwood, et al., 1999). The energy content is mainly a function of the propellant composition, which corresponds to the type of propellant (i.e., SBP, DBP, or TBP). The energy release is controlled by the burning rate of the propellant. This is determined by the chemical and physical characteristics (composition, density, mechanical strength, etc.) of the propellant. The morphological characteristics of the propellant grain (i.e., shape and size) control the rate at which gas is released during the ballistic cycle. perforation in propellant grains are used to control the rate of gas release and the burning time of the propellant grains (Atwood, et al., 1999). Figure 11 illustrates the ratio of exposed burning area to initial grain area $\left({A_x}/{A_0}\right)$ as a fraction of the grain consumed (Z) of several shapes of propellant grains. Propellant grains which burn with $\left({A_x}/{A_0}\right)$

< 1 are considered digressive. Those which have slopes of $\left({}^{A_x}/_{A_0}\right) \approx 1$ are considered neutral, and those having slopes of $\left({}^{A_x}/_{A_0}\right) > 1$ are considered progressive.

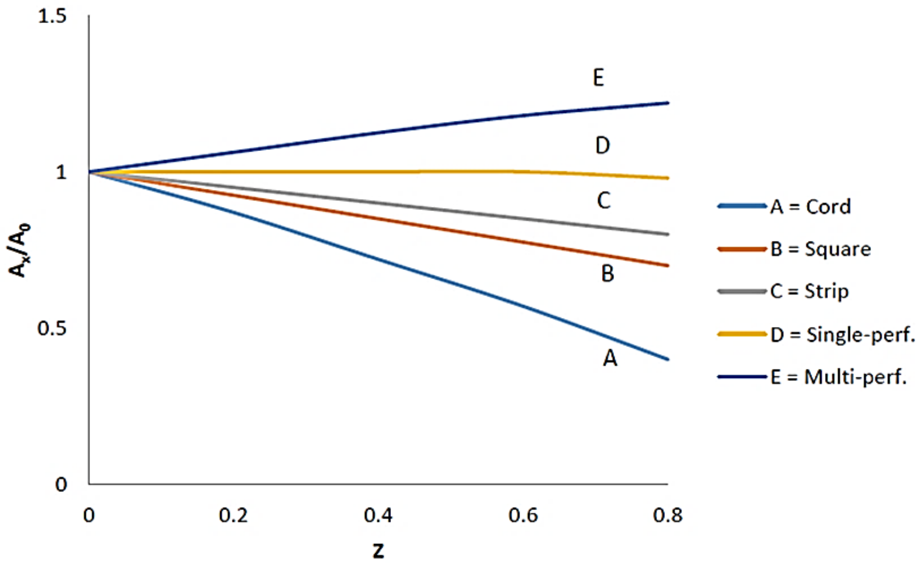

Figure 12: The ratio of the exposed burning area to the initial grain area (Ax/A0) versus the amount of grain consumed (Z) of propellant grains of various shapes (RDM, internal ballisticians, 2016).

2.4 Burnt fraction

Figure 13 shows the fraction of the grain surface area vs. the fraction of grain volume during the burning process of the tubular (digressive), the single perforation (neutral), and the seven perforation (progressive) grain geometries.

When the volume regression fraction is equal to 0, the propellant has not started to burn. Furthermore, if the volume regression fraction is equal to 1, the combustion phase has reached completion (Carlucci D. J., 2007).

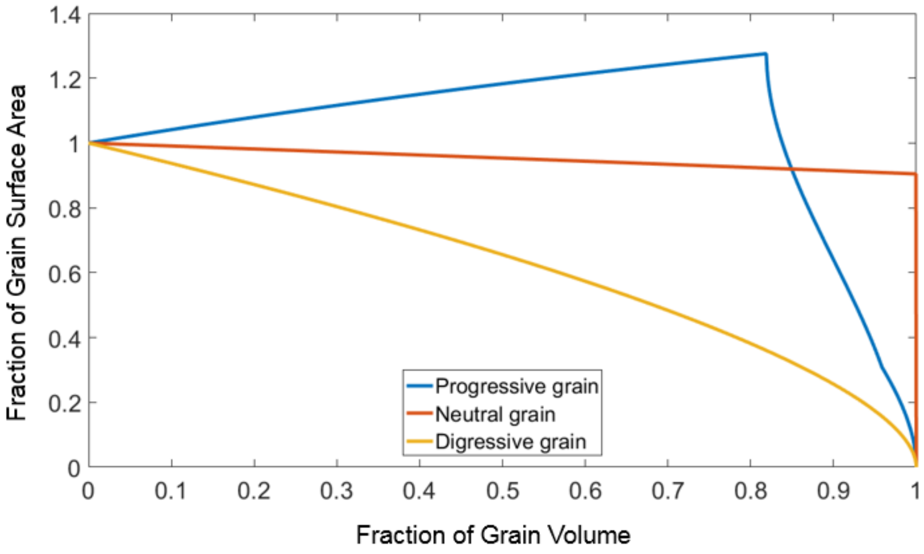

Figure 13: Grain surface area progression vs. grain volume regression (RDM, internal ballisticians, 2016).

As illustrated by Figure 13, the maximum fraction of the digestive grain's surface area occurs at the initial burning phase. The peak of gas production is consequently at the beginning of the combustion cycle. As the surface area diminishes, the gas generation of digressive grains decreases.

The surface area of a progressive grain increases with the development of the combustion process. The peak surface area of the progressive grains is reached when the grain volume regression fraction is between 0.7 and 0.8.

The surface area fraction for neutral grains is nearly constant during the combustion procedure.

2.5 Web Optimization

The propellant grain geometry determines the propellant gas delivery rate and the resulting pressure inside the gun chamber. The web size of the grains plays vital role in maximum chamber pressure as well as the muzzle velocity (MV) of the gun system.

Work done by Funday yildirim (YILDIRIM, TİRYAKİ, & KABAK, 2012) helped to establish the most applicable web sizes of grain geometries for a large calibre propellant. An adapted version of the Bear-Frankle IB model was used to replicate the IB cycle inside a gun barrel. They were able to vary the web sizes of propellant grains to determine the effect of web sizes on muzzle velocity. Figure 14 clearly shows this relationship between web thickness and muzzle velocity as the web size increases, the muzzle velocity decreases and vice versa. As a consequence, this exercise is to find the optimal match for the modified propellant grain in terms of muzzle velocity and the web size grain.

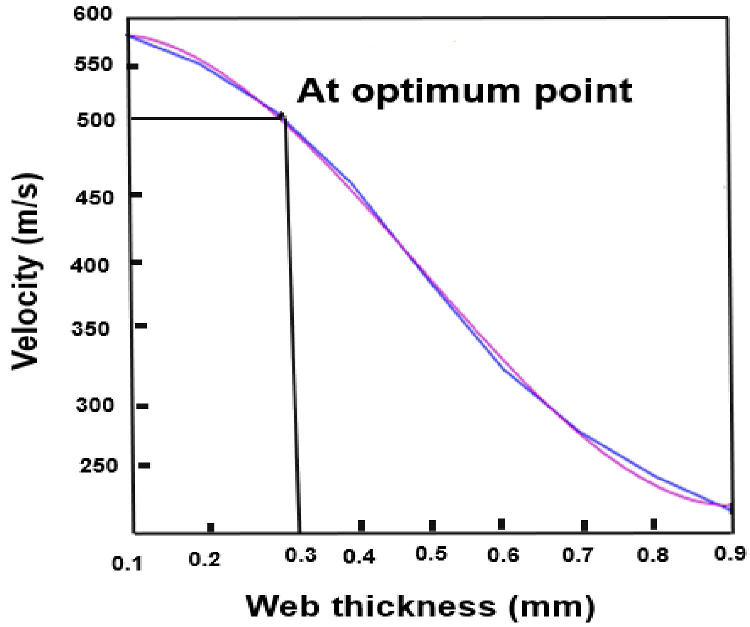

Figure 14: Muzzle Velocity vs. web thickness

The web thickness is the most vital consideration for designing the shape of a propellant grain. According to Funda yildirim, Tola and Nikbay, his is determined by two things: perforation diameter and grain diameter. The muzzle velocity increases when the pressure value of the web thickness decreases (YILDIRIM, TİRYAKİ, & KABAK, 2012) and (Tola & Nikbay, 2018). However, this only applies when the propellant size is unchanged. When symmetric perforations are present, the value of the web thickness would be correspondingly reduced. Additionally, the investigation shows a clear correlation between web sizes and the pressure inside the gun chamber. As the web size increases the pressure inside the gun chamber decreases and vice versa. When the web is relatively large, the propellant takes longer to burn thus Gas generation is slower, which flattened the pressure peak inside the gun chamber. Figure 15 shows the relation between web size and chamber pressure:

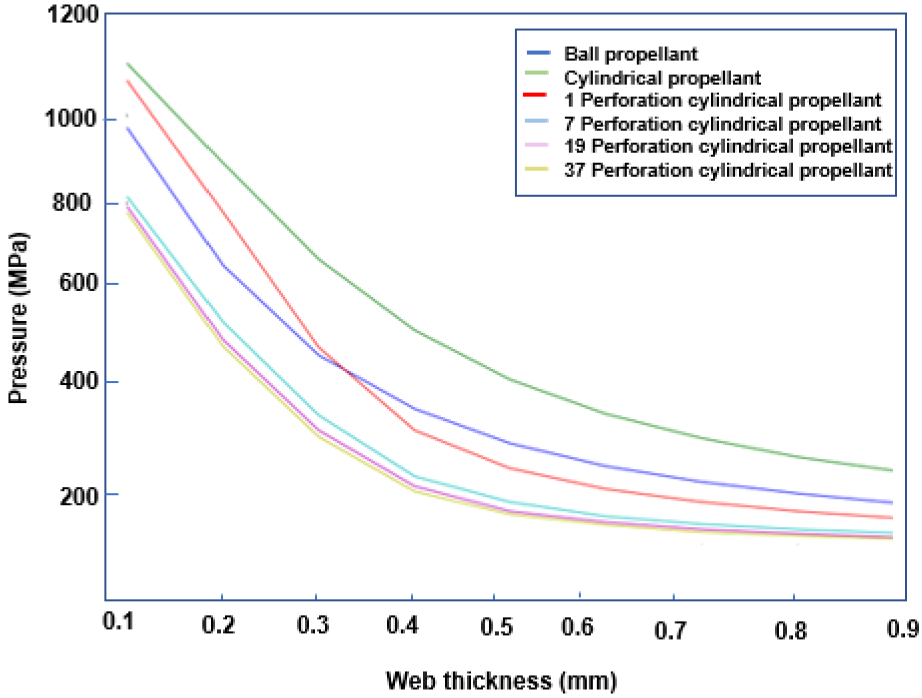

Figure 15: Chamber Pressure vs. Web thickness (YILDIRIM, TİRYAKİ, & KABAK, 2012)

2.5.1 Perforations

The interior surface area of grain increases more rapidly compared with the rate at which the outer surface decreases, for the combustion rate to increase as burning progresses, since there are a number of perforations, as shown in Figure 16 (White K. J., 1997). The maximum combustion rate will be rapidly attained after ignition if a grain is digressive. A decreasing rate follows once this maximum rate is attained. The maximum combustion rate takes place after some time with a progressive grain.

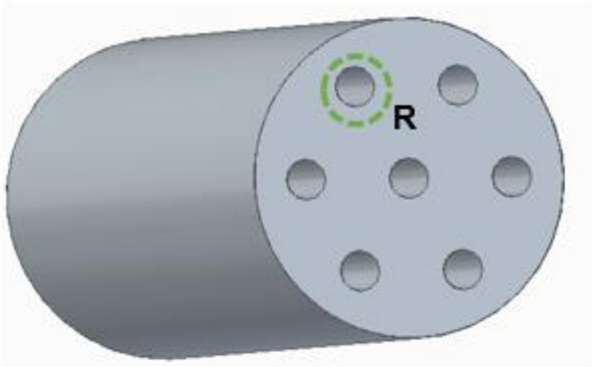

Figure 16: perforation (R = distance burned)

A propellant grain with a large number of perforations does not necessarily achieve a higher performance than a smaller sized propellant with a lower number of perforations, because ballistics relies primarily on the quantity of combustion gases produced during firing. Additionally, a higher number of perforations will burn more quickly and will not necessarily achieve a progressive curve.

2.5.2 Slivering

Slivers form residues inside the gun chamber which can affect and shorten the service life of the weapon. Slivers are created due to propellants not burning completely. This means that the gas pressure value inside the chamber is less than required or planned for. This affects the muzzle velocity negatively. Unburnt propellant sometimes gets expelled from the muzzle, which is classified as unclean combustion. When slivers are produced, this is likely to decrease the IB performance. It is possible to determine the shape of the slivers by using the offset function (Schabort, 2016). Offset function is a built in function in 3-D modelling programs. It gives the ability to simulate the burning regression of propellant grain. As a result, possible formation of slivers can be visualised.

With regards to the burning of the propellant internally and perforation, the diameter of the burning will widen from inside until it reaches the burned propellant from the outside. Pandey, 2013, in his examination of a star-shaped grain of propellant, Figure 17, shows that the inner triangular perforation will start burning from inside through the grain and become larger. Under these conditions the inner angles of the perforation will change shape to be an arc during burning (Pandey, 2013).

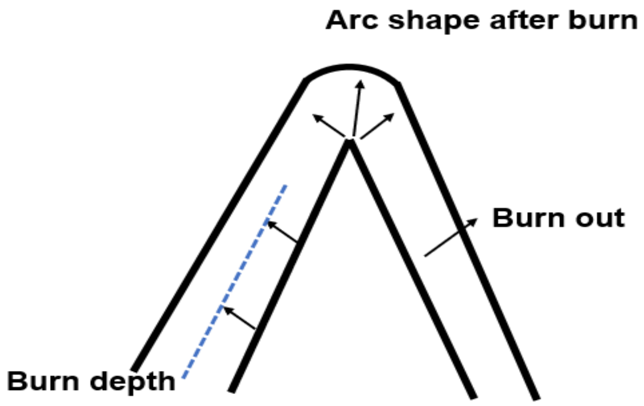

Figure 17: The sharp angle of the perforation disappears as the star shape grain evolves (Pandey, 2013)

2.5.3 Propellant web optimisation

The main aim of the web optimisation is to determine the optimum web size of a given propellant grain geometry that yields the lowest pressure for a required velocity.

2.5.3.1 Web optimisation procedure

Web optimisation should be performed for any new geometric design as follows (Schabort, 2016):

1. Select the reference grain and specify a system target velocity (for example, 945 m/s is the muzzle velocity of 155mm artillery system). All propellant options should yield this velocity.

2. Perform an IB simulation and make sure the ballistics are calibrated to the reference ballistic values (velocity and pressure).

3. Keep the resistance curve the same for all further calculations and perform all simulations to reach the same velocity.

4. Select the first alternative geometry and perform simulations:

    a. Adjust the average ballistic size (web size) to a small value (for example, 1.8 mm) and run the simulations by changing the propellant mass until the required velocity is obtained—record the mass and pressure.

    b. Increase average web size incrementally (for example 0.1mm) and perform simulations again – record the mass and the pressure.

    c. Repeat until the web size reaches the practical maximum

5. Tabulate the values and draw a graph of propellant web size (x-axis), pressure (left y-axis) and mass (right y- axis)—remember velocity should be constant Figure 18 .

6. Make observations and assess the potential performance parameters of the propellant grain design in relation to the reference propellant grain.

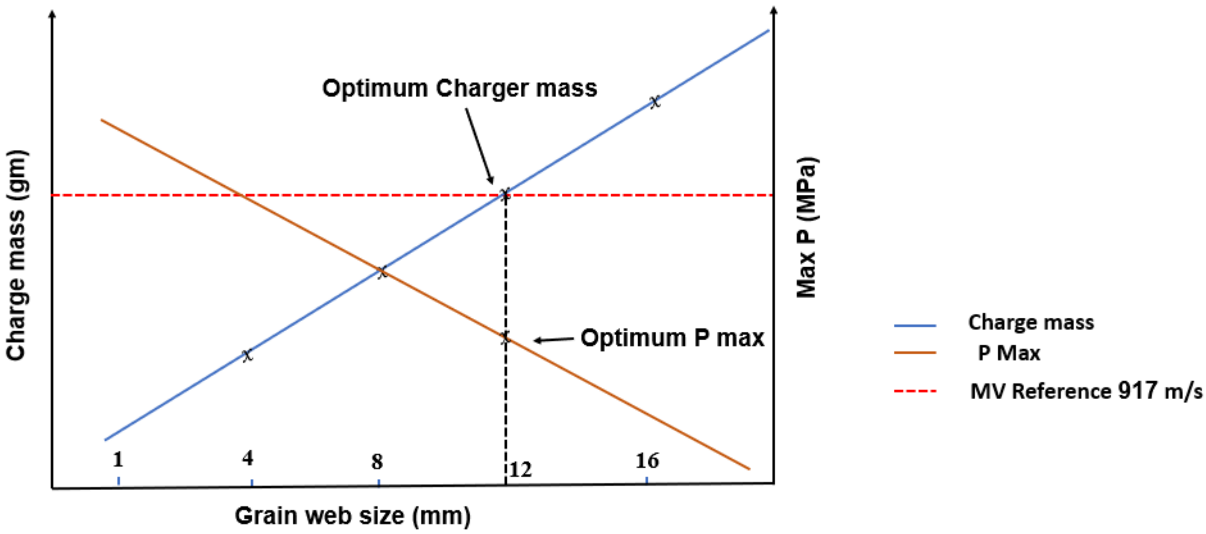

Figure 18: Web optimisation

2.6 Packing density

If propellant grains have a high packing density, they occupy a smaller volume. A smaller occupied volume means a smaller charge case, which results in a smaller gun chamber requirement. Another advantage of propellant grains with a high packing density is the improved passage of gases generated during ignition. Consequently, it is preferred to have a propellant charge with a high packing density to increase the muzzle velocity and decrease maximum pressure. This will make firing safer (Li & Zhang, 2011).

The United States of America Patent No. US4094248A, 1977 presents a high packing density propellant grain. Figure 19 shows the longitudinally grooved polygonal extruded hexagonal geometry. It provides nearly full utilisation of the circular volume of a combustible case. This illustrates that this design aims to provide high packing density, which minimises ullage in a weapon’s chamber. Furthermore, it eases the passage of gases generated during ignition. Thus, it can be seen that there are numerous advantages of having propellant grains with a high packing density (The United States of America Patent No. US4094248A, 1977).

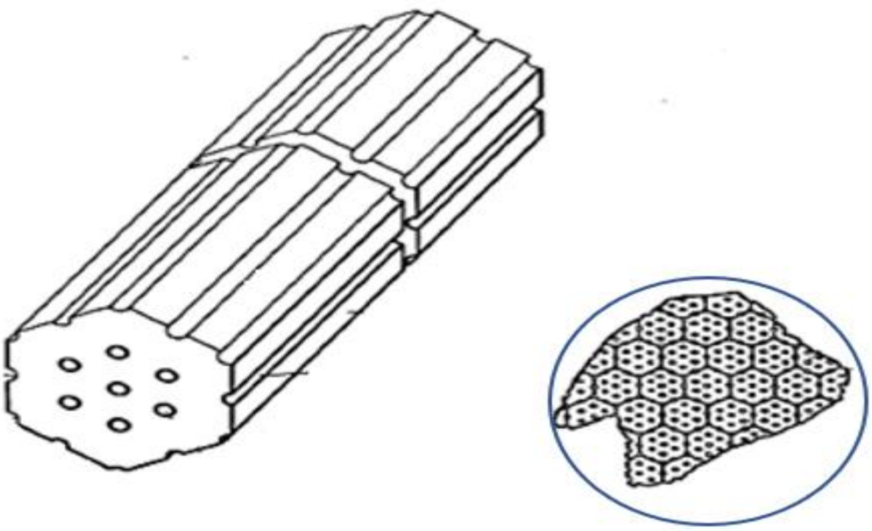

Figure 19: high packing density propellant grains

2.6.1 Modular charge system

Indirect firing artillery systems such as 155 mm artillery use the modular charge system (MCS) as the propulsion system of choice. It is incrementally based and contains several distinct combustible cases (known as charges or zones) uniquely bound together. Each case is filled with varying amounts of propellant. The range of the projectile can be customised by manipulating the number of charges in the chamber of the system. Increasing the number of charges increases the muzzle velocity of the projectile, which increases the range. When the MCS is tuned with the elevation angle of the barrel. It offers a wide range of coverage. However, MCS requires complex igniting devices to ensure optimal ignition. If the igniting system fails it could lead to the formation of an axial pressure wave which might destroy the system (Minor, 1985).

Figure 20 shows a typical example of a standard Charge module of MCS for the 155 mm heavy artillery system (Ruth, Minor, & MD., 1985). The number of charges per system normally ranges from one to six charges. Standard Charge module is an element of the MCS Each charge module consists mainly of triple-base propellant grains and combustible with a cylindrical case.

Figure 20: Standard Charge C502 modular charge system

2.6.2 Commercial nesting packages for performance testing

In previous studies the analysis of packing problems has been primarily conducted using industrial data rather than commercial nesting packages. Two commercial nesting software packages will be used for this research. They are TruNest software and MyNesting software. Using the two nesting software packages provides an opportunity to establish consistency of results and to reduce the margin of error.

2.6.2.1 MyNesting software

MyNesting is a software application that specifically assess different particle arrangements to determine space usage. MyNesting offers a wide range of features that support a better understanding of the packing environment In addition it contains different algorithms that are formulated in 2D. Due to these features, software developers and other data technicians consider it as one of the best options when writing their code. This software gets data from external sources, examines it and outputs a result. MyNesting can be used for a wide range of analytics, including sheet metal cutting fitting of patterns in different materials and most importantly in nesting of packaging material.

2.6.2.2 TruNest Software

TruNest software is another very useful application in this research. Similarly to MyNesting it is used to perform analytical procedures in different mechanical situations. It contains a library comprised of standard shape geometric objects. These objects can be analysed to establish different characteristics. Importantly it is possible to analyse a packing scenario for different shapes that are contained in the library. While using this packing analysis tool, a task can be nested either manually or automatically. If the exact packing does not exist in the library one can form it manually. The results obtained in this analysis are presented using a table that contains packing efficiency.

2.7 Conclusion

In this chapter, the burning configuration of the propellant as well as the burning rate were described in details. This chapter also explains the web optimisation of the propellant grain and its criticality during propellant grain designing. It also highlights the procedure that will be followed during web optimisation. In addition to that, it describes the programs which are going to be used to analyse the packing density of the new propellant grains. This chapter illustrates the modular charge system which is used for the 155mm artillery system.

Chapter 3: LUMPED and VERIFIED IB MODEL of STANAG 4367

3.1 Introduction

The lumped parameter model is used to simulate the interior ballistic cycle of the gun system. It is preferred because it gives an accurate solution for any internal ballistic system. It then provides predictions that are used by manufacturers of the components of these systems. The working procedure of an internal ballistics LPM involves the ignition of the propellant charge which produces propellant gases the energy of which is calculated the gas is then generated according to the pressure-gradient model the motion model then tabulates the acceleration velocity and displacement of projectile the final step of the process. This chapter describes all these processes in detail in conjunction with the equations and calculations involved.

The final part of the chapter looks at the verification process for the internal ballistic model, which has to comply with STANAG 4367, which is the standardised LPM created by NATO, and be verified against the RDM simulation program.

3.1 LPM of STANAG 4367

As the current model used for accurate and efficient internal ballistic calculations (Schabort, 2016) a benefit of LPM becomes evident when it simulates a ballistic system it gives a solution to the entire internal ballistic system. The result is the prediction of values for the manufacturers of ballistic systems, propellants and ballisticians (Dyckmans, Lumped Parameter Model, 2015).

These predictions include the following:

1. Barrel exit time.
2. Barrel exit pressure.
3. Maximum chamber pressure.
4. maximum projectile kinetic energy.
5. Burn time of the propellant.
6. Ballistic system efficiency.
7. Projectile muzzle velocity.
8. Maximum acceleration of the projectile.
9. Gun backward velocity (due to recoil).
10. Maximum pressure time.
11. Maximum wall temperature of the bore.
12. Maximum gas generation from propellants

13. Maximum pressure of the base of the projectile.
14. Maximum spin rate of the projectile.
15. Duration time of the IB cycle.

The LPM consists of several sub model that are lumped together. These sub-models are:

- The model of motion,
- The combustion model,
- The model of state,
- The energy model,

Figure 21 provides a representation of the internal ballistics LPM. The loop indicates the cycle calculations that are repeated until all the conditions are met.

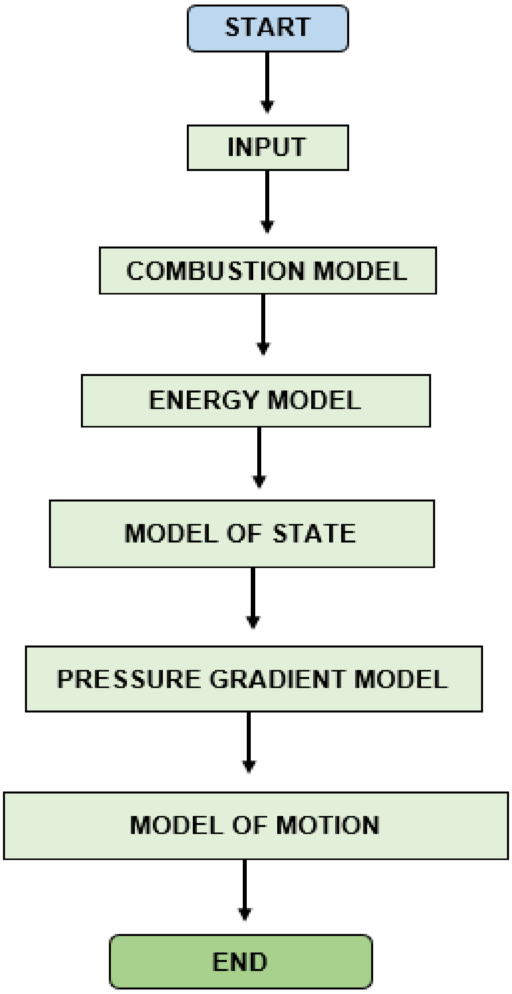

Figure 21: Flowchart of LPM of internal ballistics

The combustion model assumes the propellant charge is ignited and solves for the propellant charge combustion. After this, propellant gases are generated including some solid masses.
The calculation of the energy present in the propellant gas is made by the energy model.

The state model calculates the space-mean pressure in the gun chamber and supplies it to the pressure gradient model.

The pressure exerted on the projectile base and the gun breech is calculated by the pressure gradient model.

The motion model solves for the acceleration, velocity and displacement of the projectile and gun.

Each of the above-mentioned models according to STANAG 4367 are described in more detail in the subsequent sections.

3.1.1 Combustion model

This model calculates the amount of gas generated by the propellant grains after ignition. The model has various equations including the equation of the fraction of propellant mass burned the burning rate equation the equation for the fraction of propellant mass burning rate and the equations for form functions. The burning rate of the propellant grains is determined by the following factors:

1) The propellant's chemical composition—the inclusion of energetic materials like nitro-glycerine increases the burning rate so that it is faster than those propellants without the materials.
2) The surrounding pressure of the grain— Russell, 2009 explains that "It is universally accepted that the higher the pressure, the greater the heat transfer onto the surface of the grain and hence, the higher the rate of burning" (Russell, 2009). The higher the surrounding pressure is, the higher the burning rate is. There is a slower burning rate when the surrounding pressure is low. Vielle's law is an equation that describes the burning rate of the propellant, r. The constants in the equation are β and α, which depend on the chemical composition of the grain. The space-mean pressure of the gun chamber is represented by ($\bar{P}$).

$$r = \beta(\bar{P})^{\alpha}$$

Source: adapted from (NATO, 2009)

Equation 3-1

However, there is a need to know how the grain burns. Piobert's law states that "burning of propellant grains takes place by parallel layers where the surface of the grain regresses, layer by layer, normal to the surface at every point" (Russell, 2009). This means that propellant grains exhibit linear burning behaviour. As propellants digressively burn, they burn from all directions and retain their geometrical shape until dissipation. Piobert's law is still applicable even if the propellant grain is less than one millimetre in diameter (Russell, 2009). Consequently, when a spherical propellant grain starts to burn digressively, it burns layer by layer from all directions whilst maintaining its spherical shape until it completely disintegrates. Figure 22 shows an example of how a spherical grain maintains its geometrical shape throughout burning. It is easy to see that the total surface area of the grain shrinks while its geometrical shape is retained.

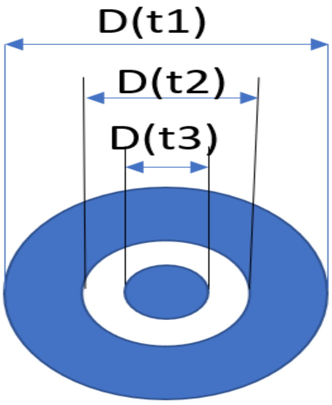

Figure 22: Burn progress (spherical grain)

Where:

$t1$ normal dimension.

$t3$ smallest dimension.

There is a rate at which gas is generated as the burning of the propellants progresses. The surface area of the propellant grains determines this rate of gas generation. Some parameters are essential for the calculation of the amount of gas generated. These include the volume of the propellant grain and the surface area of the exposed grain. The combination of the model with form functions helps to derive the total gas production. Form functions refer to analytical questions essential to the calculation of the volume and the surface area of the grain. The form functions of the spherical grain are:

$$V = \frac{1}{6}\pi(D)^3$$

$$S = \pi(D)^2$$

Source: (NATO, 2009)

Equation 3-2

Where:

V Grain volume.

D Grain diameter.

Sr Grain surface area.

To calculate the burned distance, the rate of burning is integrated. The form function is also used to update the volume and surface area of the propellant grain. Equation 3-3 below represents the rate of the mass fraction burning:

$$\frac{dZ}{dt} = \frac{Sr}{V_g}$$

Source: adapted from (NATO, 2009)

Equation 3-3

Where:

$\frac{dZ}{dt}$ Mass fraction burning rate of the propellant grain.

Sr Grain surface area.

V_g Initial volume of the propellant grain.

By integrating the mass fraction burning rate of the propellant grain, the mass burned fraction can be calculated. The mass burned fraction is thus represented as:

$$Z = \int_0^t \dot{Z}\, dt$$

Equation 3-4

Where:

Z the fraction of mass burned of the propellant equation.

The mass burned fraction can be used to determine the gas amount produced by the grain. The principle of the conservation of mass is the primary principle on which the combustion model is centred. According to this principle, mass can never be destroyed or created. Mass maintains a constant value (Hall, 2018). In other words the reduction in the mass of the propellant is the same as the increase in the mass of the resulting propellant gas. The fraction of the burnt mass is essential in the calculation stage. The equation below represents the establishment of the mass fraction burned and the remaining propellant mass at any given time.

$$C_{solid} = (1 - Z) * C$$
$$C_{gas} = Z * C$$

Equation 3-5

Where:

C_{solid} Mass of solid propellant grains.

C_{gas} Mass of propellant gas.

C Initial total mass of propellant.

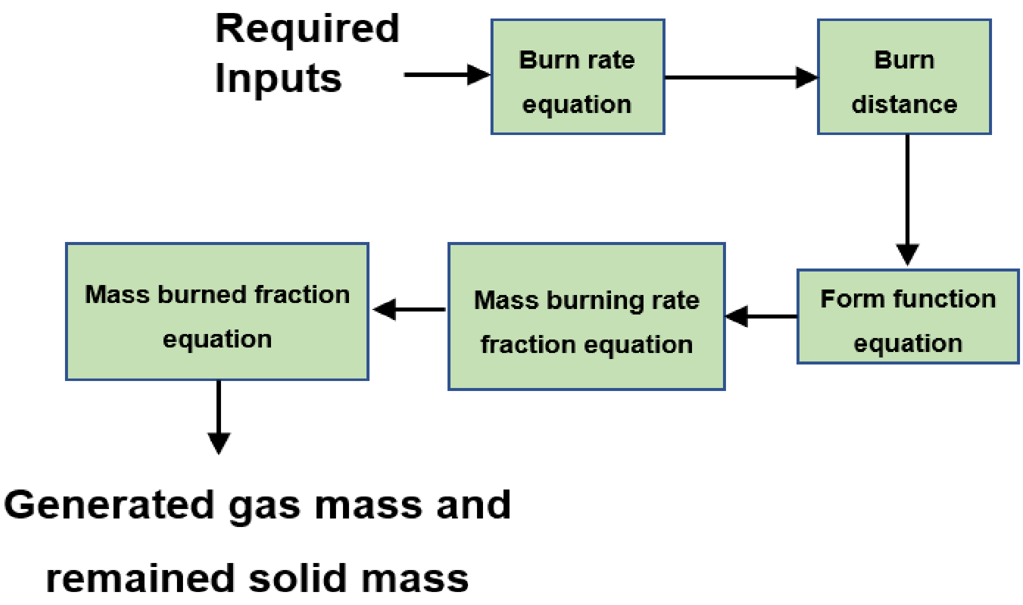

Figure 23: Combustion model flowchart

Figure 23 summarises the combustion model. The inputs required by the combustion model are the propellant grain exponents and coefficients. The inputs are processed by the burning rate equation to generate the current burning rate and burned distance. The form functions provide the capability of updating the volume and the surface area of the grains. From this update, it is easy to determine the fraction of the mass burned and the burning rate fraction. The energy model then generates the gas mass and mass of the remaining solid.

3.1.2 Energy model

The energy model is based on the concept of the conservation of energy, which stated that the total energy of an isolated system remains constant; it is conserved over time.

There is a release of hot gases in the exothermic reaction during the burning of the propellant grains. The force constant of the gases can be as high as 1200 J per gram The work-energy generated is converted into both useful and wasted energies. The energy that does not contribute to the acceleration of this energy loss. A significant difficulty faced by ballisticians is inaccuracy in the estimation of the energies (Dyckmans, Lumped Parameter Model, 2015). The expression below calculates the energy available in the propellant gases.

$$T = \frac{\sum_{i=1}^{n} \frac{F_i' \, C_i Z_i}{\gamma_i - 1} + \frac{F_I C_I}{\gamma_I - 1} - E_{pt} - E_{pr} - E_p - E_{br} - E_r - E_d - E_h}{\sum_{i=1}^{n} \frac{F_i' \, C_i Z_i}{(\gamma_i - 1) T_{0_i}} + \frac{F_I C_I}{(\gamma_I - 1) \, T_{0_I}}}$$

Source: from (NATO, 2009)

Equation 3-6

Where:

n	Number of propellants.
F_i'	Adjusted force per unit mass of i^{th} propellant.
F_I	Force per unit mass of igniter propellant.
C_I	Initial mass of igniter.
γ_i	Ratio of specific heats for i^{th} propellant.
γ_I	Ratio of specific heats for the igniter.
E_{pt}	Energy consumed due to projectile translation.
E_{pr}	Energy loss due to projectile rotation.
E_p	Energy loss due to propellant gas and unburned propellant motion.
E_{br}	Energy loss due to friction and engraving of rotating band.
E_r	Energy loss due to recoil.
E_d	Energy loss due to air resistance.
E_h	Energy loss due to heat transfer to the chamber and barrel walls.
T_{0_i}	Adiabatic flame temperature of i^{th} propellant.
T_{0_I}	Adiabatic flame temperature of the igniter.

Each of the energy losses listed above are described according to STANAG in more detail below.

1. Energy consumed by projectile translation (E_{pt}): There is a force exerted on the base of the projectile when the propellant gas moves. It increases the motion of the projectile. This translational kinetic energy derived from the total gas energy is essential for the acceleration of the projectile. This energy is 28.3% of the total energy in a 155 mm artillery system (Dyckmans, 2018). Equation 3-7 is an equation for calculating the kinetic energy of the projectile:

$$E_{pt} = \frac{m_p v_p^2}{2}$$

Source: from (NATO, 2009)

Equation 3-7

Where:

m_p Mass of projectile.

v_p Velocity of projectile.

2. Energy loss due to projectile rotation (E_{pr}): In the case where there is rifling of the bore, the projectile has both rotational kinetic energy and translational kinetic energy. In a 155 mm artillery system, the rotational energy of the projectile uses 0.4 % of the available energy (Dyckmans, 2018). Equation 3-8 calculates the projectile rotational energy:

$$E_{pr} = \frac{\pi^2 m_p v_p^2}{4T_W^2}$$

Source: from (NATO, 2009)

Equation 3-8

Where:

T_W Twist of rifling.

3. Energy loss due to propellant gas and unburned propellant motion (E_p): There is movement of unburned grains and propellant gas during combustion. An absence of the movement would result in no pressure on the projectile's base during the IB cycle. The movement uses energy. The ballistic ratio determines the energy loss, and an increase in the ratio increases the energy loss. In a 155 mm artillery system, this motion uses

2.3% of the total energy (Dyckmans, 2018). Equation 3-9 is an equation for calculating the energy loss because of the aspects mentioned above.

$$E_p = \frac{C_T v_p^2}{6}$$

Source: from (NATO, 2009)

Equation 3-9

Where:

C_T Total mass of propellants and igniter.

4. Energy lost because of engraving of the rotating band and friction (E_{br}): When the bore is rifled, the friction is enhanced; the severity depends on the barrel dimensions and materials used. The projectile needs energy to overcome this friction. The process uses 1.4% of the propellant's energy in a 155 mm artillery system (Dyckmans, 2018). Equation 3-10 describes this energy loss:

$$E_{br} = A \int_0^x P'_R \, dx$$

Source: adapted from (NATO, 2009)

Equation 3-10

Where:

A Area of base of projectile including appropriate portion of rotating band.

P'_R Adjusted resistive pressure of the bore due to friction and engraving.

The profile of the resistive pressure, as proposed by STANAG, is shown in Figure 24.

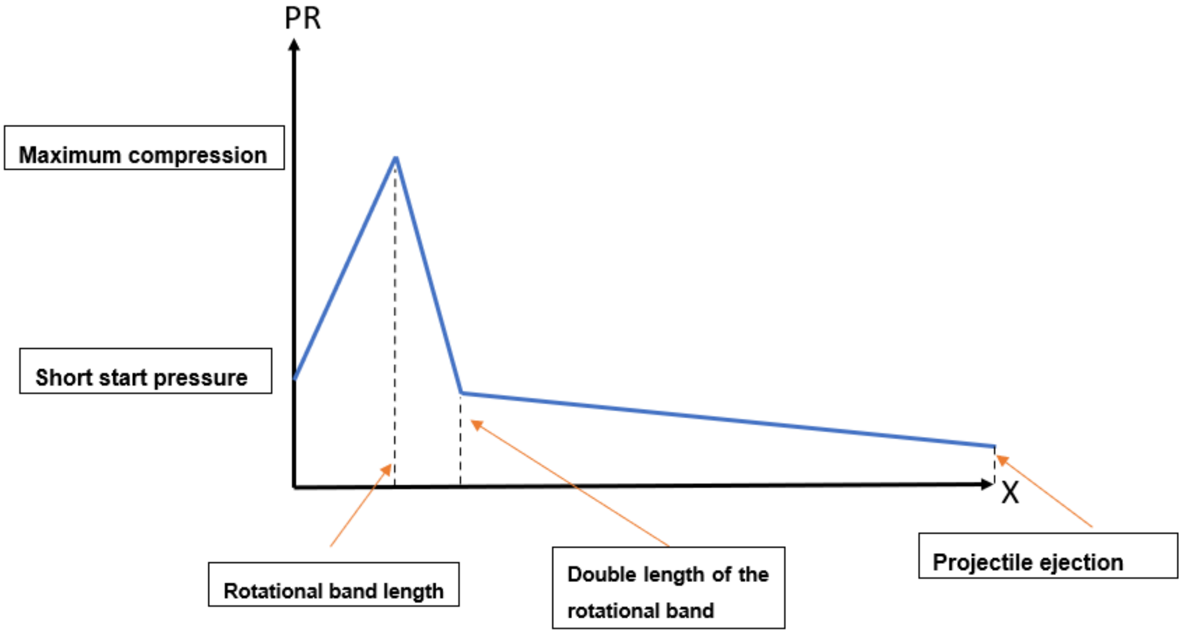

Figure 24: The resistive pressure profile due to driving band engraving and friction (Dyckmans, 2018)

Empirical evidence determines the four points that define the resistive pressure profile. The starting point of the curve is the short start pressure. It then reaches a point when the resistive pressure increases as the band occupies the forcing cone. The increasing resistive pressure comes to a maximum when it is contained by the groove. The pressure subsequently drops at the third point when the projectile is in motion. The third point is characterised by an equal distance between the length of the driving band and the distance travelled by the projectile. The fourth point, there is a constant resistive pressure from this moment up to when the driving band comes out of the muzzle.

5. Energy loss due to recoil (E_r): There is a large force on the gun breech caused by the high pressure of the gas, making the gun accelerate in the direction opposite to the projectile in the IB cycle. In a 155 mm artillery system, 1.3% of the total energy is lost in this recoil (Dyckmans, 2018). Equation 3-11 gives this energy loss:

$$E_r = \frac{m_{rp} v_{rp}^2}{2}$$

Source: from (NATO, 2009)

Equation 3-11

Where:

m_{rp} Mass of the recoiling parts.

v_{rp} Velocity of recoiling parts.

6. Energy loss due to air resistance (E_d): The acceleration of the projectile in the barrel causes air compression in front of the projectile. A resistive pressure acts on the front surface of the projectile. The projectile acceleration determines the compressed air pressure. There is a possibility of it reaching twenty times the ambient pressure. In the same scenario of a 155 mm artillery system, the energy loss is on the order of 0.1% of the total energy (Dyckmans, 2018). Below is the equation:

$$E_d = A \int_0^t v_p P_g \, dt$$

Source: from (NATO, 2000)

Equation 3-12

Where:

P_g Pressure of gas or air in front of projectile.

The pressure of the gas or air in front of the projectile can be calculated as:

$$P_g = P_a \left[1 + \alpha_a M^2 \left(\frac{1 + \alpha_a}{4} + \sqrt{\left(\frac{1 + \alpha_a}{4} \right)^2 + M^{-2}} \right) \right]$$

Source: from (NATO, 2000)

Equation 3-13

Where:

P_a Pressure in the ambient air.

α_a Ratio of specific heats for air.

M Mach number of the projectile with respect to the air.

7. Energy loss that comes from heat transfer to both the barrel walls and the chamber (E_n): The change of the propellant charges into heat is an exothermic reaction that enables the transfer of heat through radiation and convection to the cold surroundings. The heat transfer loss is the highest energy loss. Taking an example of 155 mm artillery, the loss due to heat transfer is 2.6% (Dyckmans, 2018). The energy loss equation is shown below:

$$E_h = \int_0^t A_w h(T - T_c)\, dt$$

Source: from (NATO, 2009)

Equation 3-14

Where:

A_w Chamber wall area plus the area of gun tube wall exposed to the propellant gases.

h Heat transfer coefficient of Nordheim, Soodak, and Nordheim.

T_c Temperature of the chamber wall.

As soon as the projectile moves in the ballistic cycle, there is an increase in the exposed wall area. The area of the chamber wall and the gun tube wall can be determined from Equation 3-16:

$$A_w = \frac{V_0}{A}\pi D_b + 2A + \pi D_b(x)$$

Source: from (NATO, 2009)

Equation 3-15

The heat transfer coefficient of Nordheim, Soodak, and Nordheim is calculated as:

$$h = \lambda \overline{C_p} \bar{\rho} \bar{v} + h_0$$

Source: from (NATO, 2009)

Equation 3-16

Where:

λ Nordheim friction factor.

$\overline{C_p}$ Specific heat at constant pressure of propellant gas.

$\bar{\rho}$ Mean gas density.

$\bar{v}$ Mean gas velocity.

h_0 Free convective heat transfer coefficient for air in the gun tube.

The Nordheim friction factor can be calculated as:

$$\lambda = [13.2 + 4\log(100 D_b)]^{-2}$$

Source: from (NATO, 2009)

Equation 3-17

The temperature of the chamber wall can be calculated as:

$$T_c = \frac{E_h + f E_{br}}{C_{pw} \rho_w A_w D_w} + T_{0_w}$$

Source: from (NATO, 2009)

Equation 3-18

Where:

C_{pw} Heat capacity of steel of chamber wall.

ρ_w Density of chamber wall steel.

A_w Chamber wall area plus area of gun tube wall exposed to propellant gases.

D_w Chamber wall thickness heated.

T_{0_w} Initial temperature of chamber wall.

The following figure shows the flowchart of the energy model.

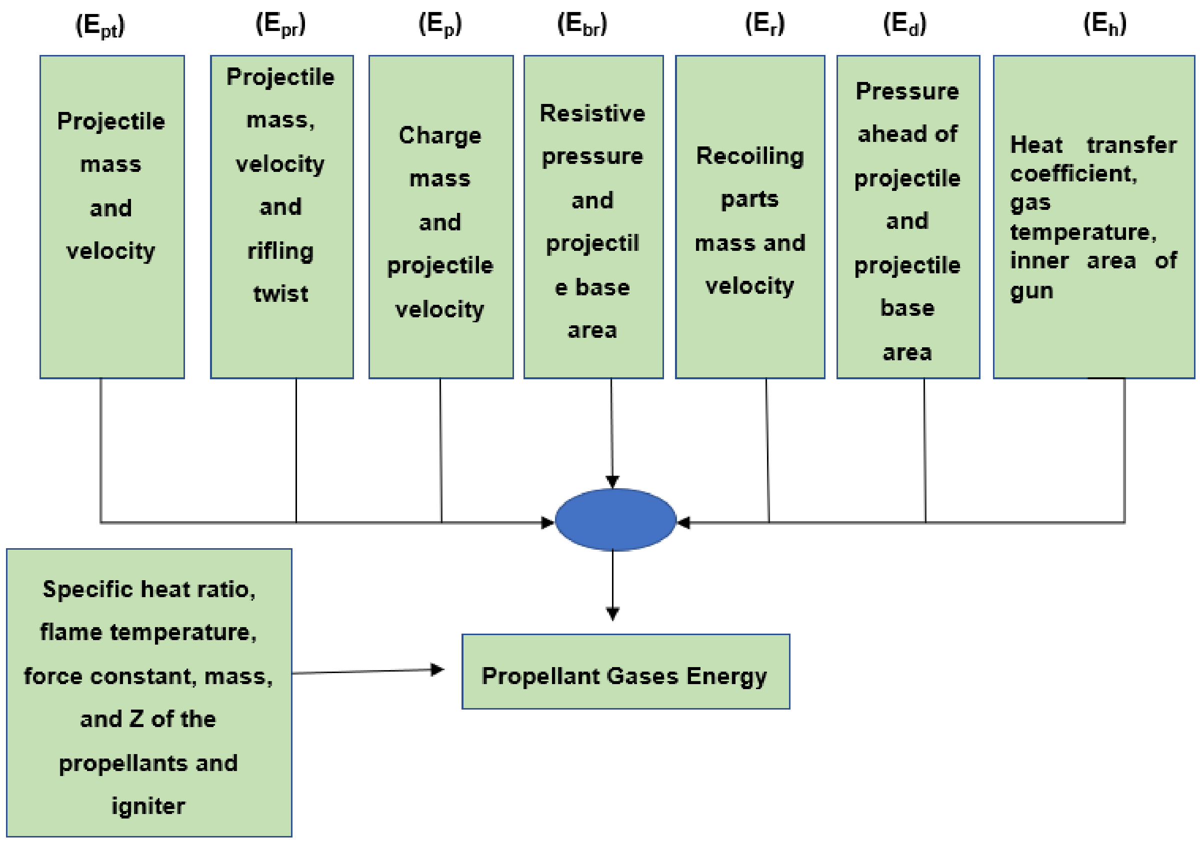

Figure 25: Energy model flowchart

After all the energy losses are calculated, the available energy in gas propellants can be calculated and applied to the state model.

3.1.3 State model

The state model computes the mean chamber pressure of the system when the propellant's gas energy is determined. The state model is based on the Noble-Abel Equation. It is important to as it describes the thermodynamic behaviour of the propellant gases. The state model is expressed as:

$$\bar{P} = \frac{T}{V_c}\left[\sum_{i=1}^{n} \frac{F'_i C_i Z_i}{T_{0i}} + \frac{F'_I C_I}{T_{0I}}\right]$$

Source: from (NATO, 2009)

Equation 3-19

Where:

V_c Volume behind projectile.

The equation calls for a value of the chamber volume, which is not constant in a ballistic system because of projectile motion and propellant charge combustion. Movement by the projectile increases the chamber volume. The volume is also increasing when the propellant charge is reduced. Figure 26 shows the effect on the chamber volume of volume enlargement in the cycle. (V_c) is the total chamber volume after projectile displacement and (V_0) is the initial chamber volume. (V_c-V_0) is the chamber volume enlargement on account for projectile displacement.

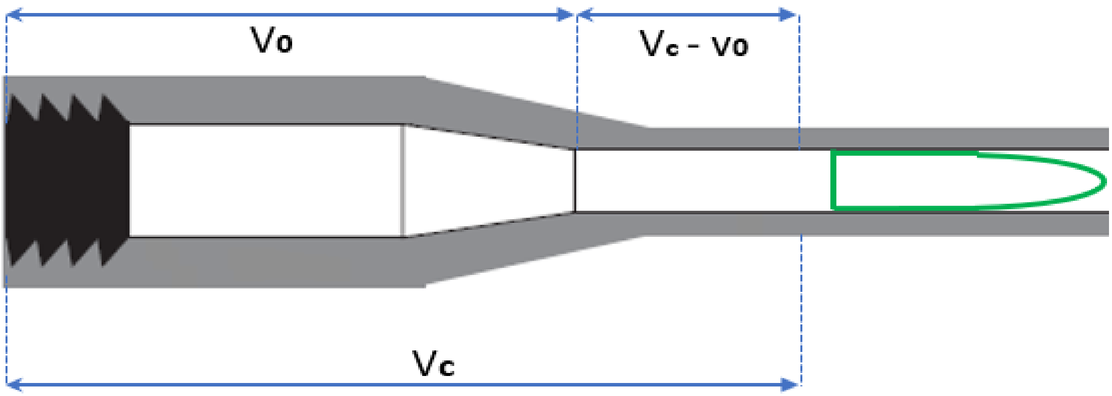

Figure 26: Chamber of ballistic system

The equation that is used to update the chamber volume during the IB cycle is expressed as:

$$V_c = V_0 - \sum_{i=1}^{n} V_{P_i} + Ax - \sum_{i=0}^{n} \frac{C_i}{\rho_i}(1 - Z_i) - \sum_{i=0}^{n} C_i b_i Z_i - C_I b_I$$

Source: from (NATO, 2009)

Equation 3-20

Where:

x Distance travelled by the projectile.

V_0 Volume of empty gun chamber.

V_{P_i} Volume of parasitics associated with i^{th} propellant.

ρ_i Density of i^{th} propellant.

b_i Covolume of i^{th} propellant.

b_I Covolume of igniter.

Figure 27 shows the flowchart of the model of state.

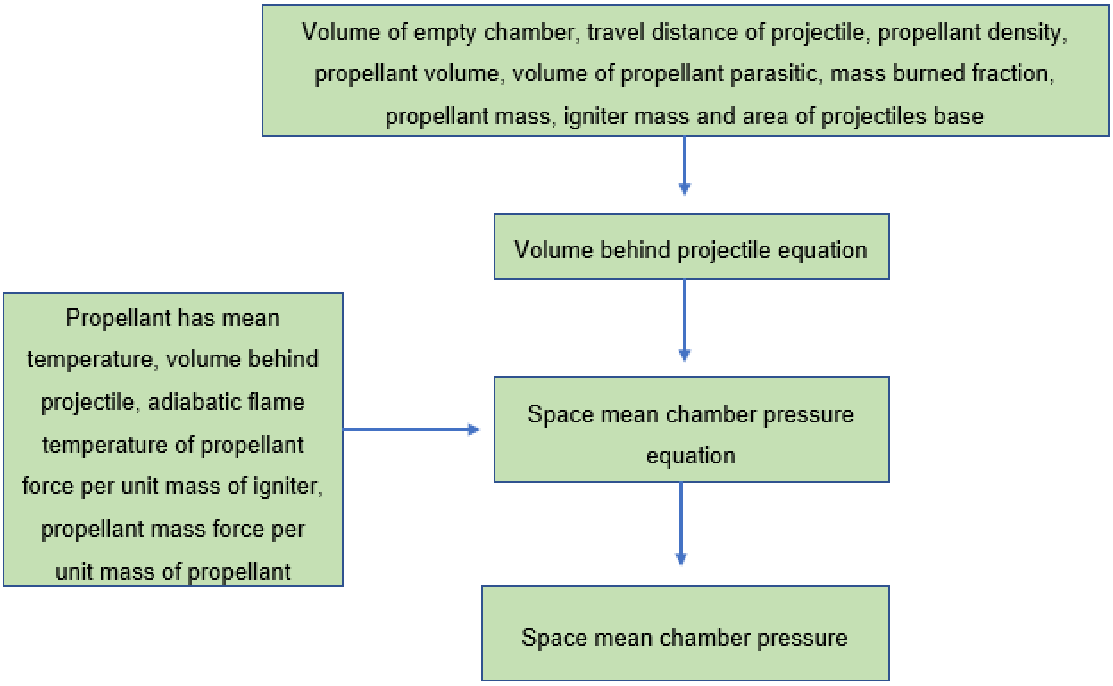

Figure 27: Flowchart of model of state

It is important to update the chamber volume before calculating the space-mean pressure. After the calculation, the Noble-Abel equation is used to determine the space-mean pressure in the chamber.

3.1.4 Pressure gradient model

There is an expansion pressure wave formed as the projectile accelerates. The wave goes towards the breech, which reflects it back as a refraction wave. The base-to-breech pressure ratio at this point is one. This ratio reduces as soon as the refraction wave touches the projectile base. The result is reduced acceleration and kinetic energy of the propellant gases. This process is continuous throughout the cycle. The pressure at the breech is higher than the pressure at the base of the projectile (Luděk Jedlicka, 2007). Figure 28 is an illustration of the gradient which occurs during the cycle.

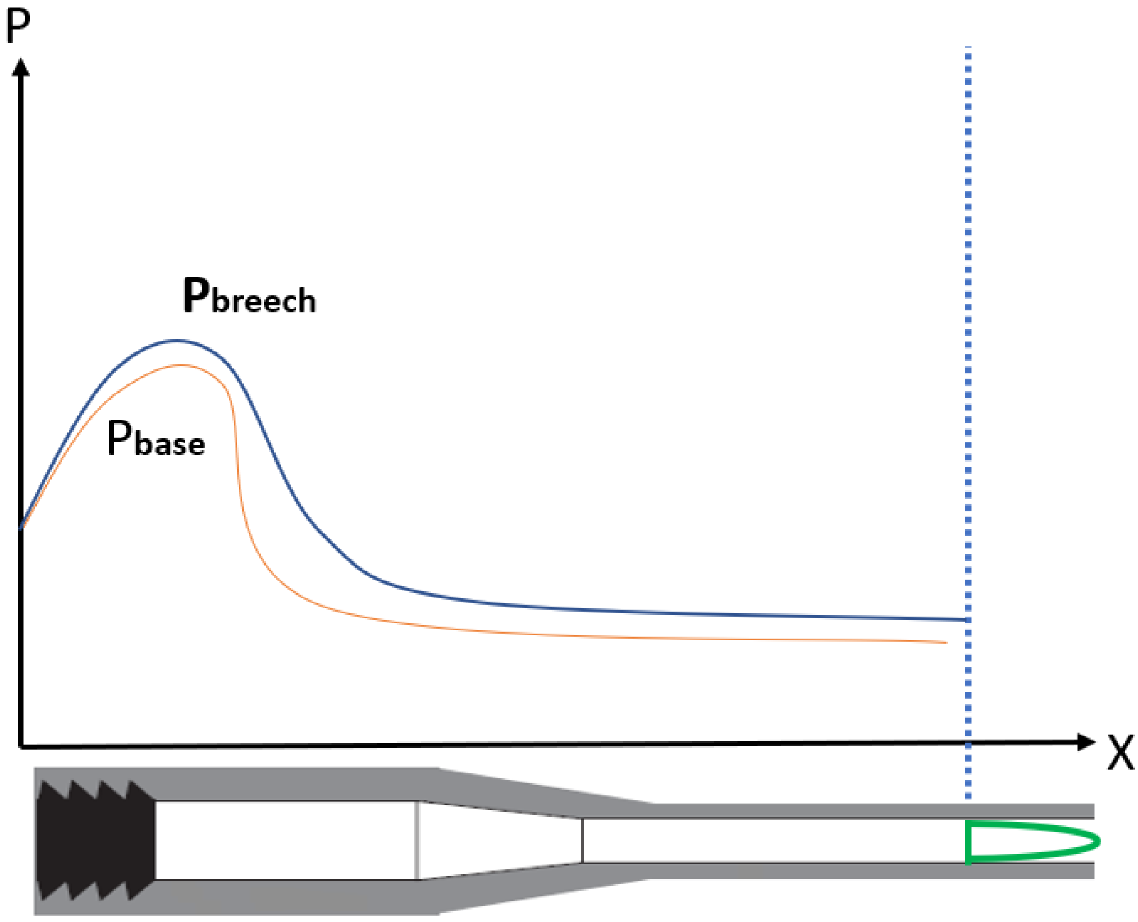

Figure 28: Pressure gradient profile

The Lagrange gradient model is a well-known model amongst ballisticians. It solves the Lagrange ballistic problem, which refers to the problem of a piston being pushed by gases under excessive combustion. Morrison suggests that the model has an assumption that the gas density between the projectile base and the breech is uniform (Morrison, Wren, Oberle, & Richardson, 1993), which causes a linear distribution for the gas velocity. Another assumption of the model is that the propellant is continuously burned before the projectile moves. It also assumes that the system's diameter is the same as the diameter of the barrel. The model also depends on the ballistic ratio, which is different from the trajectory of the projectile. It is applicable where the ratio is small. The model, which considers the relationship between breech pressure and base pressure, is presented below.

The pressure on the base of the projectile (P_b) including the approximate pressure-gradient effect is:

$$P_b = \frac{\bar{P}}{1 + \frac{\varepsilon}{3}}$$

Source: from (Morrison, Wren, Oberle, & Richardson, 1993).

Equation 3-21

Where:

ε Ballistic mass ratio

The ballistic mass ratio (ε) is:

$$\varepsilon = \frac{C}{m_p}$$

Source: from (Morrison, Wren, Oberle, & Richardson, 1993).

Equation 3-22

The breech pressure (P_0) is:

$$P_0 = P_b\left(1 + \frac{\varepsilon}{2}\right)$$

Source: from (Morrison, Wren, Oberle, & Richardson, 1993).

Equation 3-23

The Lagrange gradient model has some shortcomings. It does not take into account that there is resistive pressure experienced by the projectile because of friction and the driving band engraving. It also does not consider the effects of air compression that cause a resistive pressure on the projectile. An improvement of the model takes into account the resistive pressure and the air pressure in front of the projectile (NATO, 2000) (Anderson, 1987). Below is the improvement on the Noble-Abel model:

The pressure on the base of the projectile (P_b), including the approximate pressure-gradient effect, is:

$$P_b = \left[\bar{P} + \frac{C_T(P_g + P'_R)}{3m_p}\right] / \left[1 + \frac{C_T}{3m_p}\right]$$

Source: adapted from (NATO, 2000)

Equation 3-24

Where:

P_g Pressure of gas or air ahead of projectile.

The breech pressure (P_0) is:

$$P_0 = P_b + \frac{C_T}{2m_p}\left(P_b - P'_R - P_g\right)$$

Source: from (NATO, 2000)

Equation 3-25

Figure 29 shows the flowchart of the pressure gradient model.

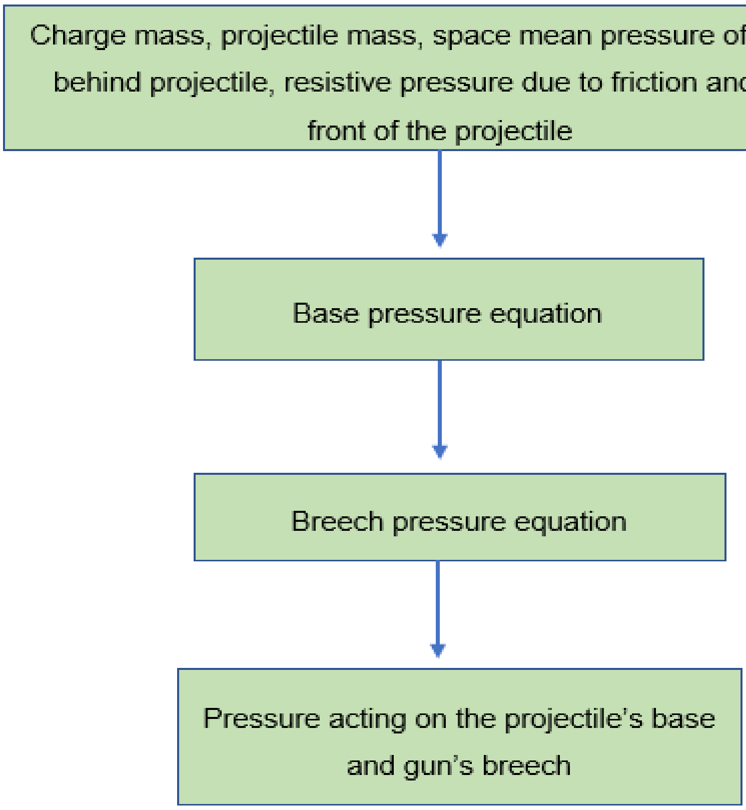

Figure 29: Flowchart of pressure gradient model

After the calculation of the space-mean pressure, the pressure on the base of the projectile is calculated by the base pressure equation. The estimate of the pressure on the gun's breech is calculated by the breech pressure equations.

3.1.5 Model of motion

Model of motion helps in determining the displacement, velocity, and acceleration of the gun during the cycle. Forces build up on the breech of the gun and the base of the projectile when the propellant charge is ignited, causing the projectile to accelerate forward. Newton's Second Law governs the model of motion. It states, "the rate of change of momentum of a body is directly proportional to the net forces applied, and the change in momentum takes place in the direction of the applied dominant force". Figure 30 shows the forces on the projectile.

Figure 30: Net forces acting on the projectile and the gun

The orange arrows show the net forces on the gun. The forces are a result of resistive pressure and breech pressure. The equation below expresses the centre of mass of a recoiling gun (Moreno, 2009):

$$\dot{\boldsymbol{v}}_{\boldsymbol{rp}} = -\frac{A_{br}P_0 - AP'_R}{m_{rp}}$$

Source: adapted from (NATO, 2009)

Equation 3-26

Where:

A_{br} Area of breech face.

The negative sign represents the direction of motion. It is easy to calculate the displacement and the gun velocity after calculating the acceleration. V_{rp} represents the velocity of the gun recoil and it can be calculated using Equation 3-27 below:

$$v_{rp} = \int_0^{t_r} \dot{v}_{rp}\, dt_r$$

Source: from (NATO, 2009)

Equation 3-27

Where:

t_r Recoil time

v_{rp} Velocity of the gun recoil

The displacement of the gun recoiling (x_{rp}) in the earth reference frame is calculated as:

$$x_{rp} = \int_0^t v_{rp}\, dt$$

Equation 3-28

The red arrows indicate the forces acting on the projectile. The causes of the forces include the resistive pressure caused by friction and the air in front of the projectile and the base pressure. Figure 30 indicates the direction of every force. The equation below represents the equation of acceleration of the center of mass of the projectile (Moreno, 2009).

$$\dot{\boldsymbol{v}}_{\boldsymbol{p}} = \frac{A(P_b - P'_R - P_g)}{m_p}$$

Source: from (NATO, 2009)

Equation 3-29

Where:

$\dot{\boldsymbol{v}}_{\boldsymbol{p}}$	Acceleration of projectile.
P_b	Pressure on base of projectile.
f_r	Down-tube resistance factor.
P_R	Resistive pressure of the bore due to friction and engraving.
m_p	Mass of projectile.
A	Area of base of projectile including appropriate portion of rotating band.

The area of the base of the projectile, including the appropriate portion of the rotational band, is described by:

$$A = \frac{\pi}{4} D_b^2$$

Source: from (NATO, 2009)

Equation 3-30

Where:

D_b	Diameter of bore.

Measuring the bore diameter is easy if the bore is smooth. It is harder to determine when the bore is rifled because of the presence of circumferential grooves. Before presenting the equation, further explanation of rifle boring is needed. Figure 31 shows a rifled bore:

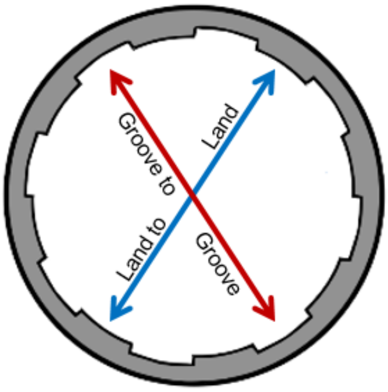

Source: adapted from (Scepaniak, 2014)

Figure 31: Cross-section of a rifled bore

The lands and grooves in the internal surface of the bore indicate its non-uniformity. The calculation of the rifled bore diameter, as defined by STANAG 4367, is:

$$D_b^2 = \left[\frac{GLR * DG^2}{GLR + 1} + \frac{DL^2}{GLR + 1}\right]$$

Source: from (NATO, 2009)

Equation 3-31

Where:

GLR Groove to land width ratio.

DG Diameter of groove.

DL Diameter of lands.

After the projectile acceleration is calculated, the velocity of the centre of mass of the projectile is given by:

$$v_p = \int_0^t \dot{v_p}\, dt$$

Source: from (NATO, 2009)

Equation 3-32

Where:

t Time.

The true travel of the projectile is calculated as the projectile travel minus the gun travel due to recoiling. The expression below represents the true travel of the projectile.

$$x = \int_0^t v_p\, dt + \int_0^t v_{rp}\, dt$$

Source: from (NATO, 2009)

Equation 3-33

Where:

v_{rp} Velocity of recoiling parts. In the earth reference frame, it is always negative.

x Travel of the projectile

Figure 32 shows the flowchart of the model of motion.

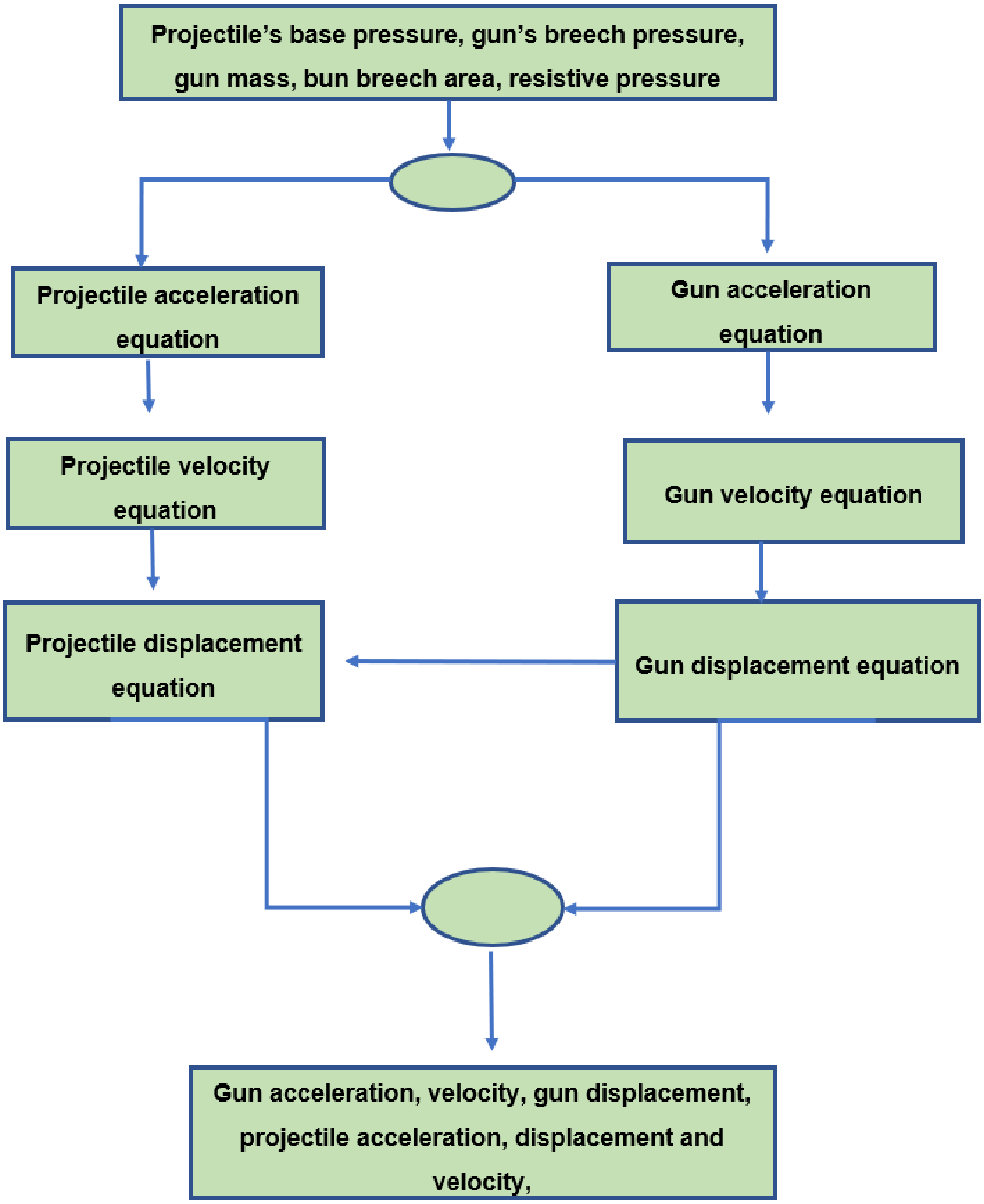

Figure 32: Flowchart of the model of motion

It is easy to determine the projectile and gun acceleration when the pressure of the gun and the base pressure of the projectile are known. Integration of the acceleration gives the velocity. It is crucial to determine the gun displacement before determining the projectile displacement. After determining this, the projectile's true position can be found.

3.2 Model verification

It is vital to verify the internal ballistic model after its development. The verification of the model is done by verifying it against the IB program of RDM. The IB program of RDM has been in service for twenty years, over which time it has seen increased effectiveness and efficiency. Product development is one area where the model is utilised fully. Testing the model includes comparing results from it to many hundreds of ballistic systems ranging from small to large calibre (Schabort, 2016).

The figures below show velocity vs time and maximum pressure vs time for rosette grain outputs from the IB model that has undergone development Figure 34 versus the results from the RDM IB model Figure 33. All the input files were identical. The result is the verification of the IB model.

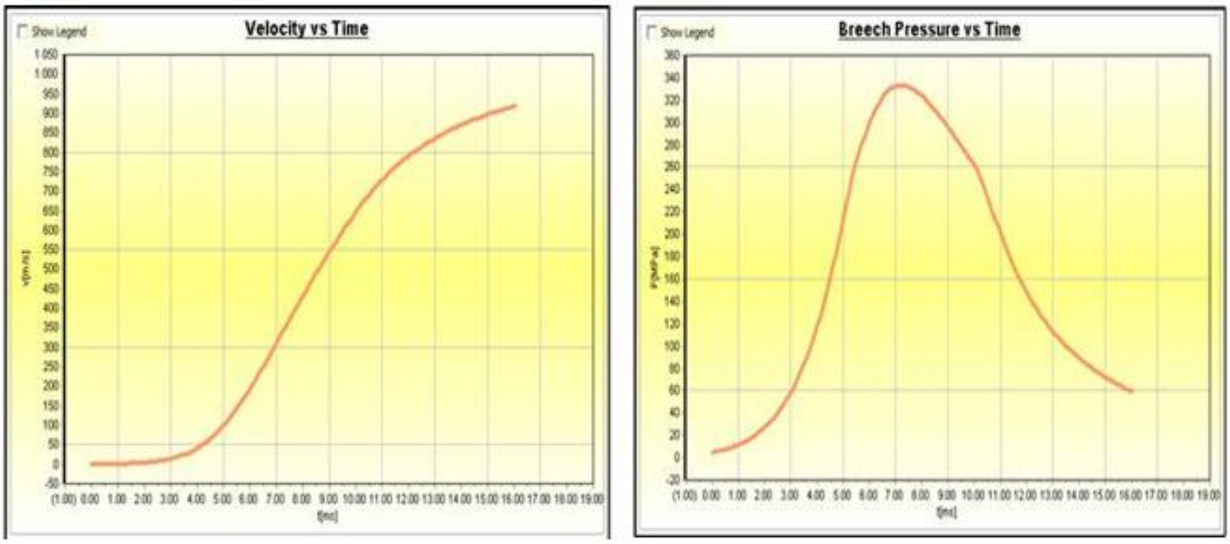

Figure 33 Output RDM IB model

The figure below shows the breech pressure curve as well as the projectile velocity curve of the developed IB simulation model . The curves are free from any sort of discontinuity and oscillation.

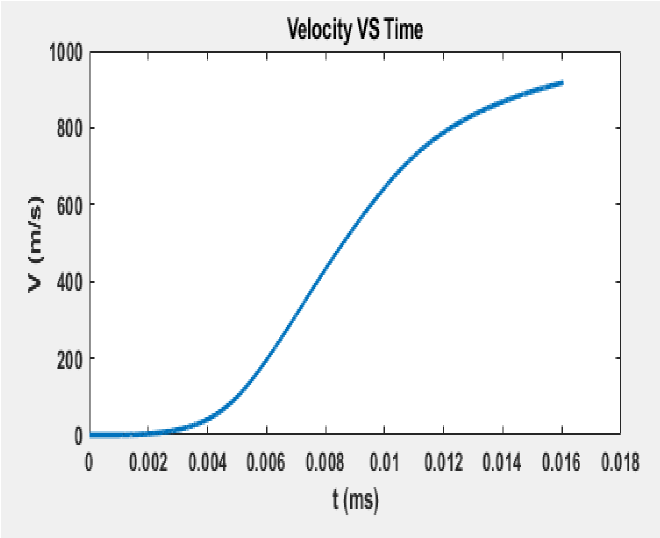

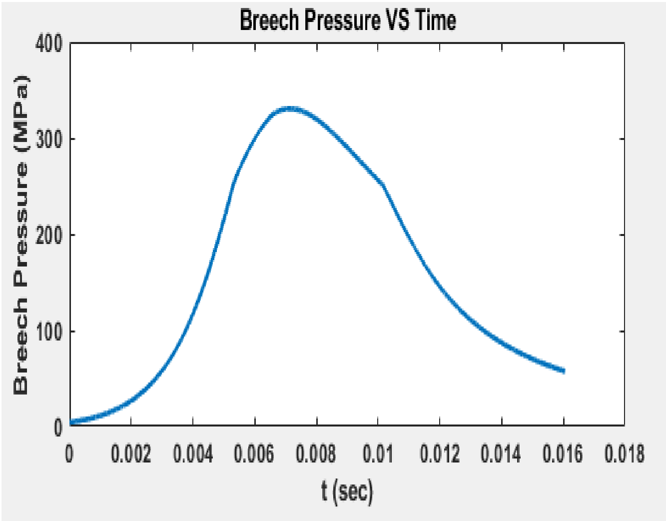

Figure 34 Output develop MATLAB IB model

The results are summarised in the following table:

Table 1: Comparison of muzzle velocity and maximum pressure between RDM model and the developed program

Internal ballistic properties **155 mm System**	**RDM** **(Reference)**	**Developed program**
Maximum Pressure (MPa)	333	330.50
Muzzle Velocity (m/s)	918	917.79

The difference between the simulations is -3.5 MPa and -0.21 m/s, within 0.77% for pressure and 0.02% for velocity.

For the purpose of this work this accuracy is entirely acceptable given that measurement accuracy is typically in the range of 2%. Due to the complexity and time-consuming nature of investigating the differences between the two simulations, pursuing a 100% match was not desirable. The verification results were deemed to be sufficient for going ahead with relative calculations using the MATLAB Code. Relative ballistic results are the focus of this investigation.

3.3 Conclusion

This chapter contains an in-depth analysis of the STANAG 4367 LPM model. The discussion touches on various aspects of the model, including the state model, the combustion model, the energy model, the equation of motion and the pressure gradient model.

Additionally, multiple assumptions are pointed out that relate to the internal ballistic LPM. Finally, the code calculates the expected results for the muzzle velocity and maximum pressure for the 155 mm system by changing the form function for the grain propellant shape. In addition, the simulation program was tested to verify whether it was fit for purpose. It was verified against the RDM model which is another internal ballistics simulation program.

Chapter 4: DESIGN

4.1 Introduction

Chapter 4 discusses a propellant grain design proposal, using the rosette propellant grain shape as the reference grain as it is the used grain in 155mm artillery system. The study entails analyses of both 2- and 3-dimensional shapes with the purpose of improving ballistic efficiency. The process of design entails using the standard procedure of developing 2D and 3D shapes, followed by web optimisation analysis.

The design process utilises parametric modelling in Solid Edge; this is used to develop the drawings. IB0D written in MATLAB is used to predict the performance of the internal ballistic propellant this involves the calculation of the vital internal ballistic properties such as the maximum pressure in the chamber and the muzzle velocity.

Furthermore, this chapter provides a detailed evaluation of the methods utilised in the calculation of the internal ballistic performance. This research is advantageous for two reasons. First, it aims to minimise and eliminate the slivers remaining after the ballistic event and consequently enhance the burning area to optimise the overall efficiency. Second, it facilitates a higher packing density for the propellant charge and uses the spaces within a propellant charge to optimise combustion efficiency.

4.2 Propellant grain design

The design process is aimed at defining a propellant grain that can facilitate the required change in pressure against time for the 155 mm artillery system while at the same time satisfying other constraints such as mass, muzzle velocity and mass charge. The propellant analysis is done in four steps that focus on independently assessing the following:

1. develop new design of the propellant grain.

2. develop a form function for the proposed propellant grain.

3. verify the form function against the off-set function of the Solid Edge program.

4. integrate the verified form function with the developed IB simulation model and simulate the 155mm artillery system with the proposed propellant grain.

5. compare the output against the 155mm artillery system with rosette grain type propellant charge.

6. finally, packing density analysis.

Table 2 lists the gun system characteristics of the 155 mm gun system; Table 3 illustrates the internal ballistic system of the 155 mm gun system and Table 4 lists the propellant systems of the 155 mm gun system.

Table 2: Reference gun system characteristic 155 mm (52 Cal)

Gun system	
Chamber volume	24182 cc
Groove length	9898 mm
Barrel length	7898 mm
Projectile mass	43500 g
Propellant mass	13522 g

Input Parameters used for the reference gun system 155 mm (52 Cal) (RDM, RDM Internal Ballistic, 2018)

Table 3: Internal ballistics system reference 155 mm (52 Cal)

Internal ballistic system	
Propellant mass	13500 g
Muzzle velocity	918 m/s
Maximum pressure	333 MPa
Barrel exit pressure	49.267 MPa

Input parameters which are used in internal ballistics simulation program to simulate the 155mm (52 Cal) artillery system (RDM, RDM Internal Ballistic, 2018).

Table 4: Reference propellant system (Rosette 7-perforation grain)

Propellant system	
Web size	2.3 mm
Outer grain diameter	10.2 mm
Length of grain	20.46 mm
Perforation diameter 1	0.40 mm
Perforation diameter 2	0.30 mm

The design of the grain geometry is done using the Solid Edge software. The software has the capability to efficiently handle parametric modelling. To ease the processing of the design, the grain is handled in parts. This is vital since it ensures minimisation of the probability of surface creation failure. To create a basic geometry, a simple variable input is enough. To create the grain geometry, various grain parameters are required. These parameters include the thickness of the grain, the outside diameter of the grain, the length of the grain, the number of perforations and the internal diameter of the grain. The stated parameters have a significant effect on variable performance. Then it is possible to accurately predict the burning rate.

To achieve the highest muzzle velocity with the lowest pressure. Firstly, a reference velocity must be specified. After that, the required mass must be established, Which will make it possible to calculate the reference velocity. It is also possible to directly specify the pressure and velocity.

4.2.1 Rosette design (reference design)

The rosette grain design originates from the multi-perforated grain and is designed to avoid the largest amount of sliver. Inner slivers formation has been found to be the main drawback of rosette designs (RDM, RDM Internal Ballistic, 2018).

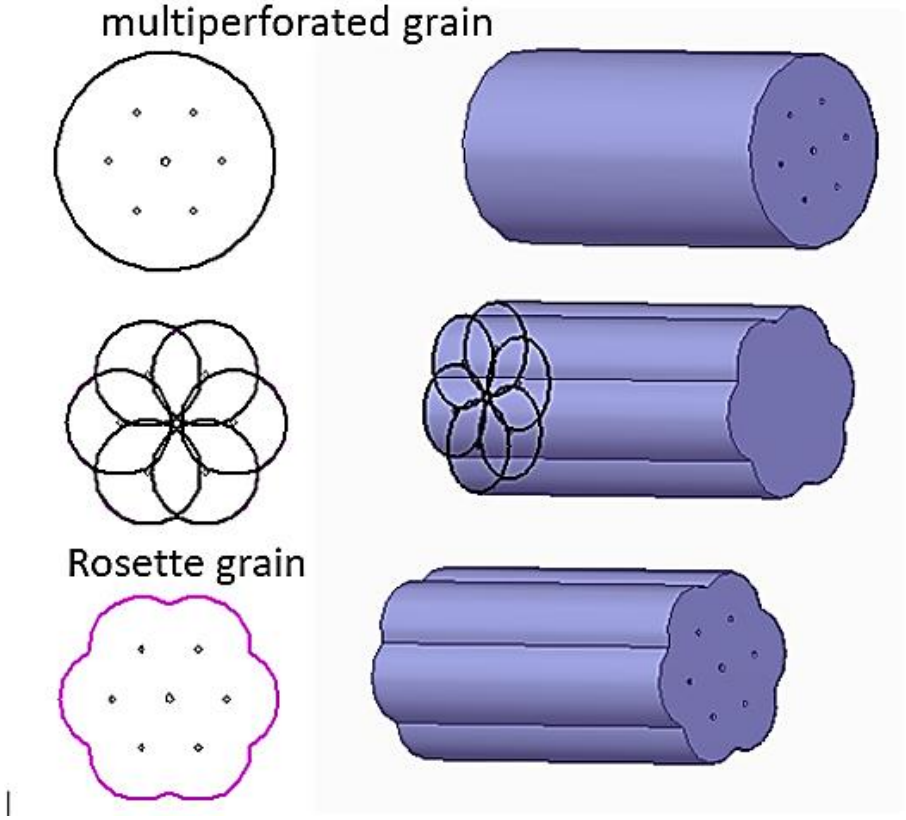

Figure 35: Sequence design rosette grain shape

Figure 35 shows the sequence of the rosette design. It started with the 7-perforation propellant in the shape of a circular cylinder and this design was modified to the rosette shape to avoid the outer slivers.

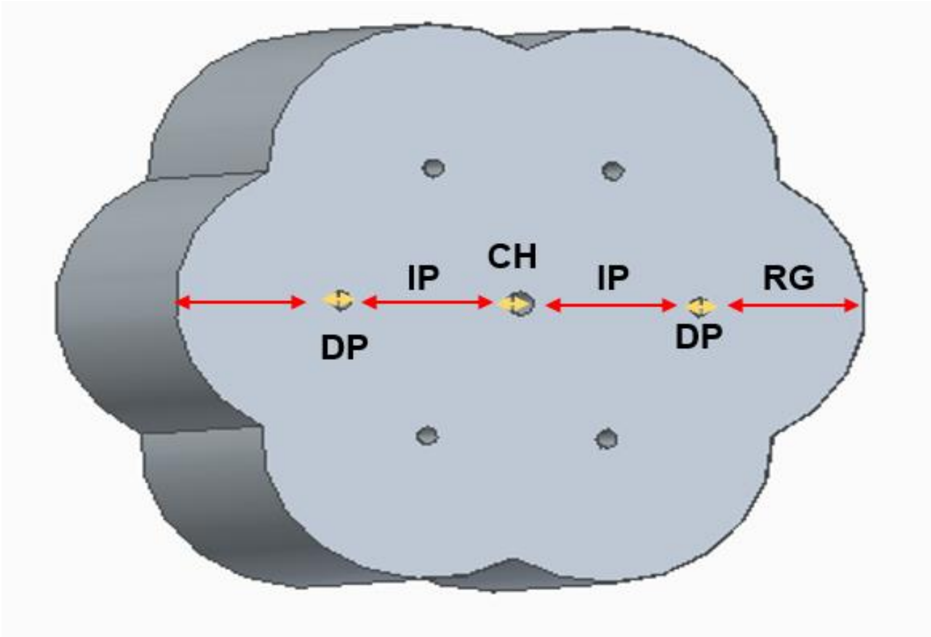

Figure 36: Schematic illustration of the rosette grain

Figure 36 (RDM, RDM Internal Ballistic, 2018) the main geometrical parameters for evaluating the propellant shapes have been introduced. Determination of the geometrical characteristics of the grain is required for evaluating the gas generation rate and after that estimating the muzzle velocity and maximum pressure.

Table 5 describes the measurements of the rosette geometry (RDM, RDM Internal Ballistic, 2018).

Table 5: Parameter input for the rosette grain

Rosette			
Grain Parameter	**unit**	**value**	**Symbol**
Web thickness	mm	2.3	IP
Outer diameter	mm	10.2	OD
Inner diameter	mm	8.712	ID
Radius of the side	mm	2.450	RG
Grain length	mm	20.460	L
Grain surface area	mm^2	73.52	Sr

Table 6 describes the measurements of the perforation of the rosette geometry (RDM, RDM Internal Ballistic, 2018).

Table 6: Parameter input perforation for the rosette grain

rosette grain **Perforations**			
Perforation Parameter	**unit**	**value**	**Symbol**
Number of perforations	-	7	p
Perforation diameter 1	mm	0.400	$DP1$
Perforation diameter 2	mm	0.300	$DP2$
Perforation Surface area 1	mm^2	0.07	$AP1$
Perforation Surface area 2	mm^2	0.13	$AP2$

4.3 Proposed propellant grain geometrical design

4.3.1 Hexa tri-perforation design

The proposed propellant grain design geometry that are investigated is a hexagonal shape which consists of six equal sides containing six perforations of triangular shape to minimise the slivering. This design is illustrated in Figure 37.

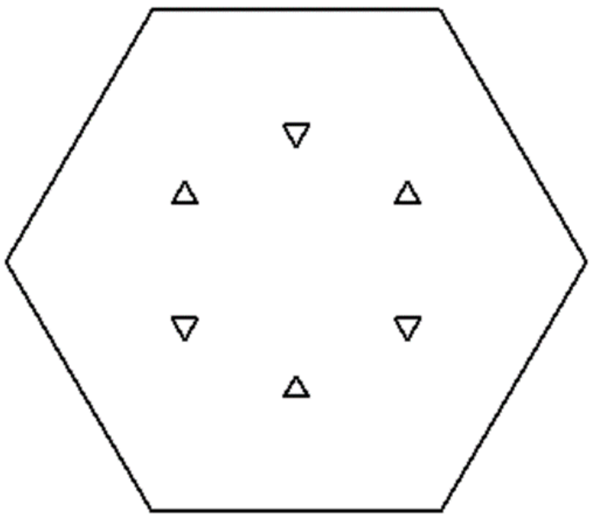

Figure 37: Hexa tri-perf propellant grain shape

Table 7 shows the key parameters of the proposed propellant grain geometric design utilised in the combustion model. Because the rosette grain is the baseline, the dimensions of the proposed propellant grain are carefully determined thus the surface area of the proposed grain is equal to the surface area of the rosette grain. This means that the amount of gas generated from the rosette grain is equal to the gas generated from the proposed grain. The surface area of the rosette grain, which is used in 155mm propellant charge is equal to 73.52 mm^2. The following table presents the dimensions of the proposed propellant grain:

Table 7: Parameter inputs for hexa tri-perf grain

Hexa tri-perf			
Grain Parameter	**unit**	**value**	**Symbol**
Number of perforations	-	6	p
Web thickness	mm	2.3	IP
Number of the side	-	6	NG
Outer diameter	mm	10.678	OD
Inner diameter	mm	9.248	ID
Length of the side grain	mm	5.339	SG
The opening angle in degree	deg	120°	θ
Grain length	mm	20.460	L
Grain surface area	mm^2	73.51	Sr

4.4 Development of the form function

The aim of the form function is to calculate the surface area and the volume for the propellant grain. The form function of the hexa tri-perf grain is as shown in Figure 38 below:

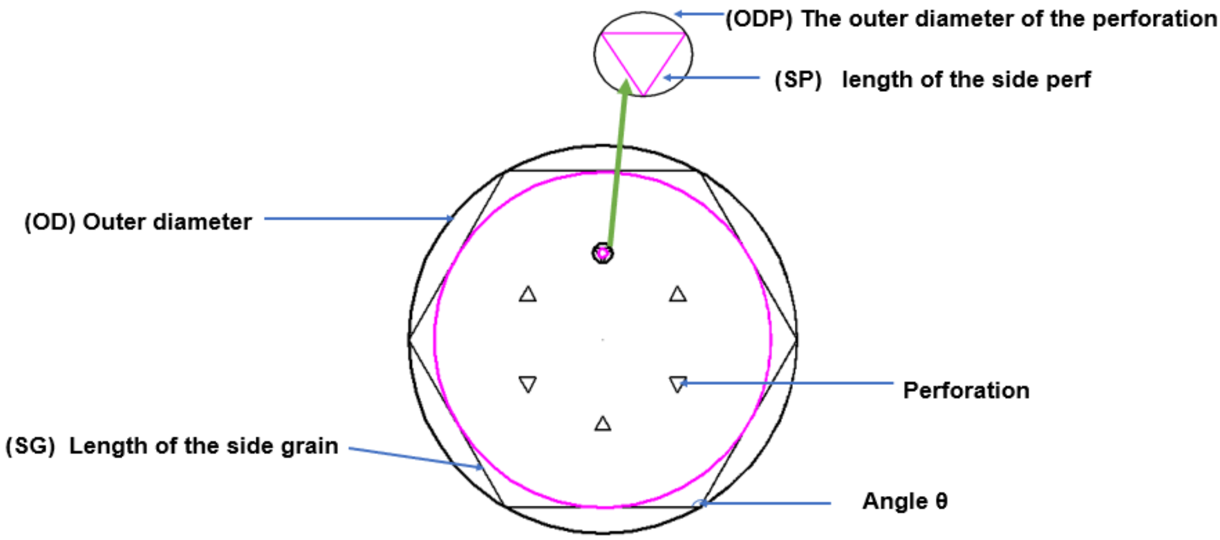

Figure 38: Hexa tri-perf propellant grain geometry

As can be seen the propellant grain is derived from polygons. The perforations are on trigon shape and the grain itself is in hexagon shape. To formulate the form function that calculate the grain surface area, mathematical equations that describes the perforation area, the upper and lower sides of the grain, and the sides of the grain have to be developed. The following is a breakdown of all the equations that when combined describes the surface area of the grain:

To calculate the surface area of the grain, the following formula will be used. However, this equation neglects the perforations. The following equation is based on regular polygon equations:

$$AGP = 0.25 * (SG)^2 * p * \left(\frac{1}{tan}\left(\frac{\pi}{p}\right)\right)$$

Equation 4-1

Where:

SG Length of the side grain.

p Number of perforations.

AGP Surface area of the grain with all perforations.

To calculate the surface area of the perforation (AP), the following formula will be used. The following equation is based on regular polygon equation:

$$AP = 0.25 * (SP)^2 * NS * \left(\frac{1}{tan}\left(\frac{\pi}{NS}\right)\right)$$

Equation 4-2

Where:

AP Surface area of the perforation.

SP Length of the side perforation.

NS The number of the side perforations.

To calculate the total grain surface area of the hexa tri-perf, the following formula will be used:

$$Sr = (AGp) - (AP * P) + (6 * L * SG) + (6 * 3 * SP * L)$$

Equation 4-3

Where:

Sr Grain surface area.

L Grain length.

To calculate the hexa tri-perf grain total volume, the following formula will be used:

$$V = Sr * L$$

Equation 4-4

Where:

V Grain volume.

After formulating the form function of the proposed propellant grain, the output of the form function has to be verified against the output of Solid Edge. After verification, the form function will be ready to be integrated within the IB simulation model.

To verify the equations, the surface area of the proposed propellant grain should be calculated using Solid Edge as well as the developed form function. In addition to that, both outputs should give an identical output.

Table 8 shows the surface area of the proposed propellant grain via the developed form function as well as the solid edge. It can be seen that the results of surface area calculations are identical, which gives an indication that the form function is correct. In addition to that, a burn distance is added to the form function as well as the solid edge program and it turns out the result are identical as can be seen from the table below. Solid edge can measure the area of the grain shape independent. In other words, it can measure the perforations independent from the whole shape.

Table 8: Verification of the form function for hexa tri-perf grain propellant

Burnt distance (mm)	Surface Area Form function	Surface Area Solid Edge	Differences (+/-)
0.00	73.51	73.51	0.00
0.002	73.54	73.54	0.00
0.462	64.34	64.34	0.00
0.924	52.95	52.95	0.00
1.386	39.34	39.34	0.00
1.848	23.52	23.52	0.00

4.5 Slivering analysis

Figure 39 shows the proposed propellant grain after applying the offset function via Solid Edge program. It simulates the burning regression of the proposed propellant grain. From the figure, it can be seen that there is a possibility of sliver formation in the centre of the grain as well as the outer edges of the propellant grain. It can be seen that, as the triangular shape perforation enlarges due to burning, the triangular shape perforation edges get rounded causing non-linear burning behaviour.

As the propellant grain burns, it will shrink while maintaining its outer shape. With regard to the burning of the propellant internally, the perforation radius always opens between two surfaces when burning from the inside, the inner triangle (perforation) angles will change shape to be arcs rather than angles during burning. The diameter of the burning will widen from the inside, reaching the burned propellant from the outside however there are points where they do not meet causing slivers.

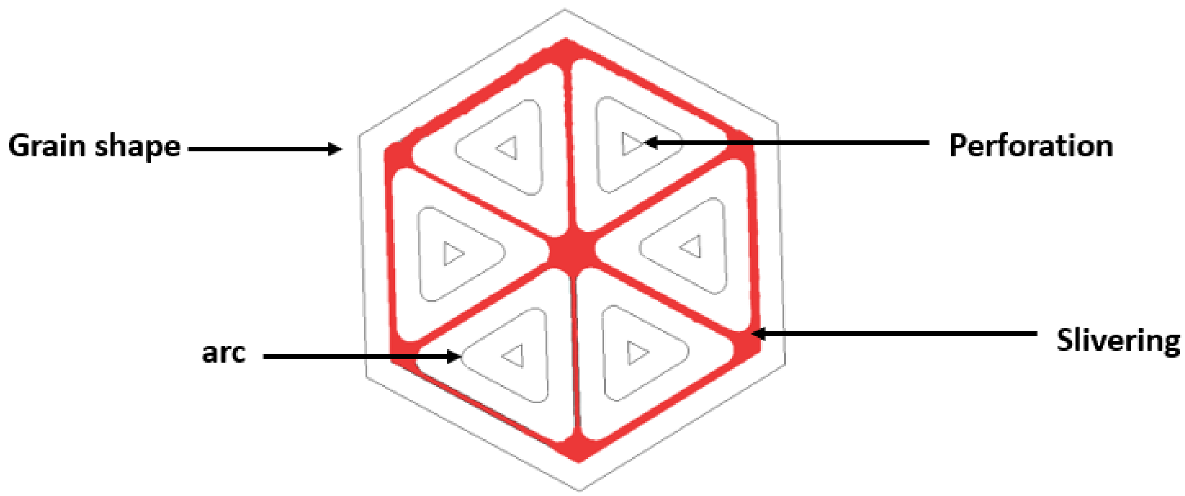

Figure 39: Determination of hexa tri-perf sliver geometry

4.6 Lumping the new propellant form function into IB Code

The following chart Figure 40 shows how to lump the hexa tri-perf propellant grain geometry form function into the IB code:

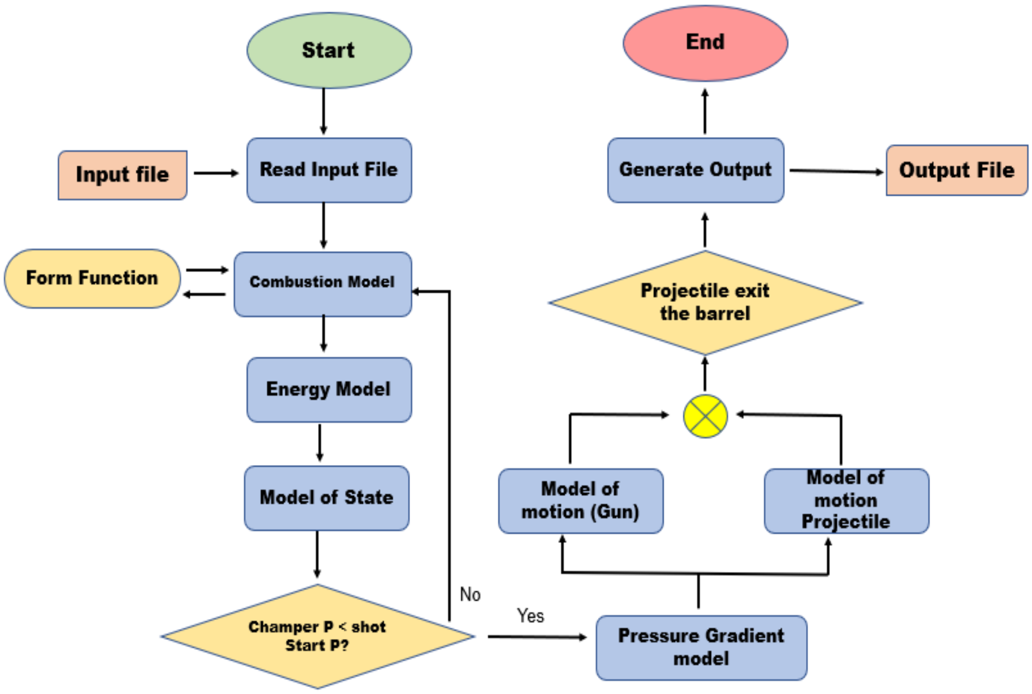

Figure 40: Flowchart of LPM of IB

1. Run the program to read the input (introduced in Tables 2, 3 and 4).
2. The form function calculates the face area and the volume of the grain shape propellant.
3. The combustion model starts and calculates the generated gas mass due to propellant burning and the remaining solid mass of the propellant.
4. The program checks the space-mean pressure is greater than the shot start and starts the pressure accordingly.
5. If the space-mean pressure is still less than the shot start pressure, the program will integrate until this condition is met.
6. Once the condition is met, the space-mean pressure is give as input to the pressure gradient model in order to calculate the exerted pressure on the projectile base and the gun breech.
7. After that the equation of motion solves the acceleration, the velocity and the displacement of the projectile and gun.

8. The projectile state is checked via the program. If the projectile exits the muzzle the outputs are generated and the program is terminated. However, if the projectile has not exited the muzzle, the program will iterate until this condition is met.

In Chapter 5 the MV and the maximum pressure will be calculated in order to compare them with the corresponding parameters for the 7-preformation rosette grain's geometrical shape that serves as the reference grain. Additionally, the web optimisation for the hexa tri-perf will be done in the next chapter.

4.7 Conclusion

In this chapter, a new propellant grain design was proposed. Also, the form function of the proposed propellant grain was formulated. The form function was verified against solid edge modelling program. After form function verification, the sliver formation analysis was carried out. Finally, the form function of the developed propellant grain lumped to the developed IB simulation model.

CHAPTER 5: RESULTS and DISCUSSION

5.1 Introduction

This chapter will present an analysis of the results obtained from the study. In addition the chapter will outline the results and explain details of the findings of the general study. The custom-developed code measured several properties of the internal ballistics, most importantly, the muzzle velocity and the maximum pressure.

In order to make an appropriate comparison between these results and the assessment of the internal ballistic cycle performance, the following parameters have been outlined and evaluated (muzzle velocity and the maximum pressure).

The chapter will use two commercial nesting software programs (TruNest and MyNesting) to verify the packing density. Moreover, a comparison between the proposed propellant hexa tri-perf, and the rosette geometry will be conducted to determine the packing density for each grain for comparative purposes.

The following are the breakdown of this chapter:

(a) Run an interior ballistic simulation of the 155mm artillery system with the proposed propellant grain and compare it to the rosette grain.

(b) run a web optimization analysis on the proposed grain to select the proper web thickness.

(c) run an interior ballistic simulation of the 155mm artillery system with the proposed propellant grain (optimized web) and compare it to the rosette grain.

(d) run a packing density analysis on the proposed propellant grain (optimized web).

Then with the evaluation of the advantages and disadvantages of the shape with regards to the reference shape (rosette with seven perforations) the study is concluded.

5.2 Hexa tri-perf propellant grains

The 155mm artillery system is simulated using the proposed propellant grain. Because the comparison is between the proposed propellant grain and the rosette grain. the propellant inputs parameter such as propellant mass as well as chemical properties were fixed.

Figure 41 shows the chamber pressure curve generated by the IB simulation program using the proposed propellant grain. the maximum pressure is equal 256.42 MPa, which is way less than expected because the maximum pressure results using the rosette grains can reach up to 333 MPa.

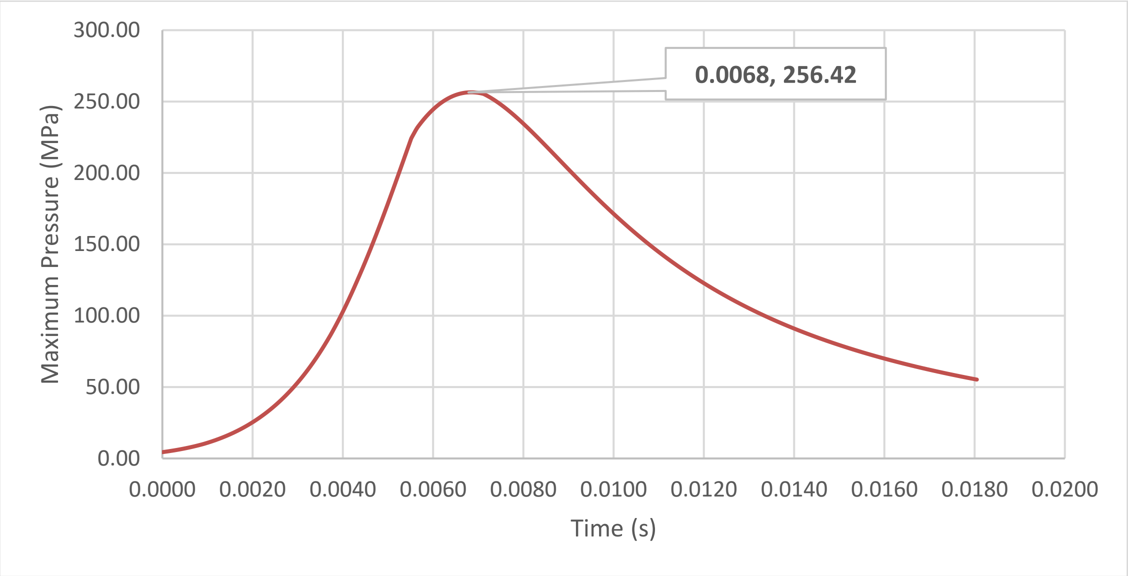

Figure 41 Pressure vs. time curve for hexa tri-perf

Figure 42 shows the projectile velocity of the 155mm artillery system after being simulated using the IB simulation program using the proposed propellant grain. the muzzle velocity using the proposed grain reaches up to 772.82 m/s, which is way less than the specifications of the 155mm artillery system, which is around 920 m/s.

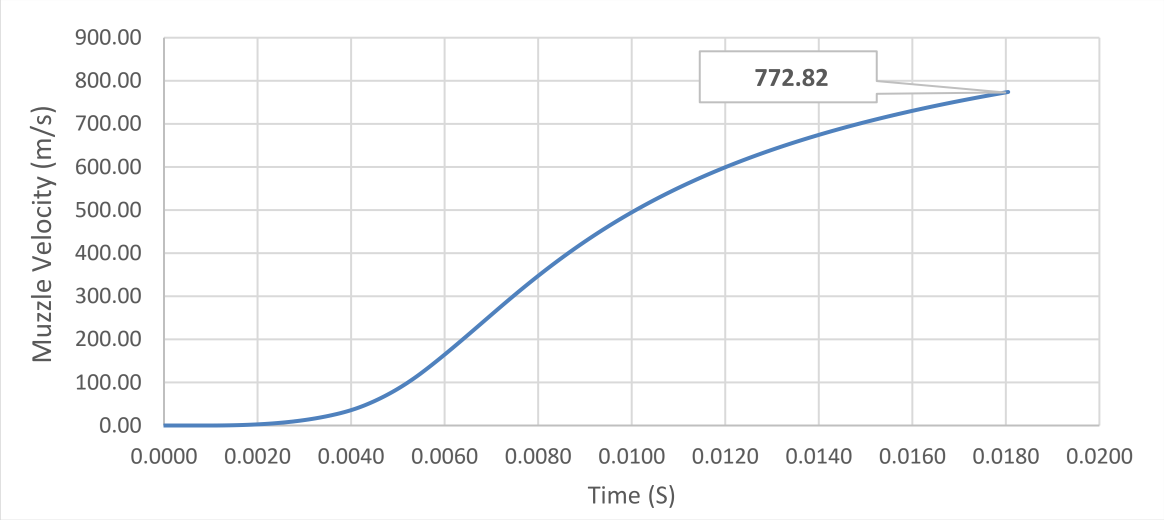

Figure 42: Velocity vs. time curve for hexa tri-perf grain geometry

5.3 Comparison of the results

The following tables presents a comparison of 155mm artillery system simulated performance between the hexa tri-perf propellant grain and the rosette grain.).

Table 9: Comparison of maximum P and MV for hexa tri-perf

Grain propellant	**maximum P (MPa)**	**MV (m/s)**
rosette (Reference)	330.50	917.78
hexa tri perf	256.42	772.82
Deviation	**74.08**	**144.96**

it can be seen that the maximum pressure of the proposed grin is less than the maximum pressure of the rosette grain by 74 MPa. In addition, the muzzle velocity achieved using the proposed grain is 772 m/s, which is less the than rosette grain by 144.96 m/s. However, after web optimisation the result might vary.

Figure 43 shows a comparison between the 155mm artillery system chamber pressure using both types of grains.

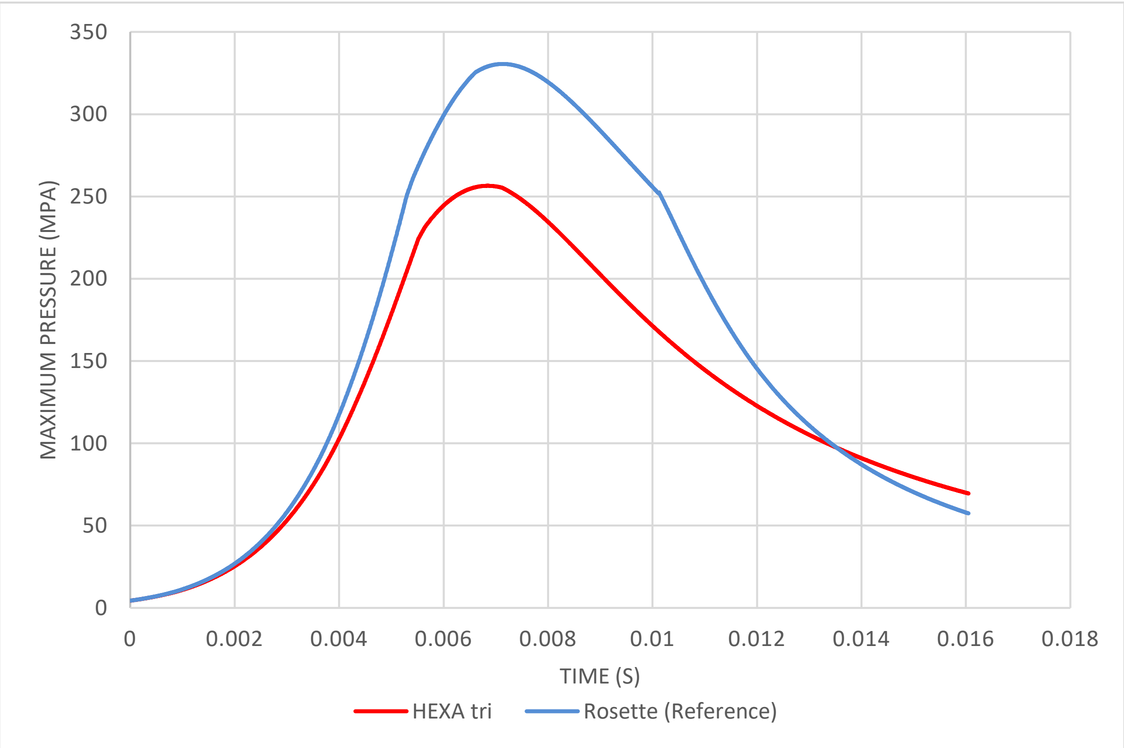

Figure 43: Comparison of the maximum P for hexa tri-perf and rosette grains

Figure 44 shows a comparison between the projectile velocity of the 155mm artillery system using both types of grains.

Figure 45: Comparison of the MV for hexa tri-perf and rosette grain

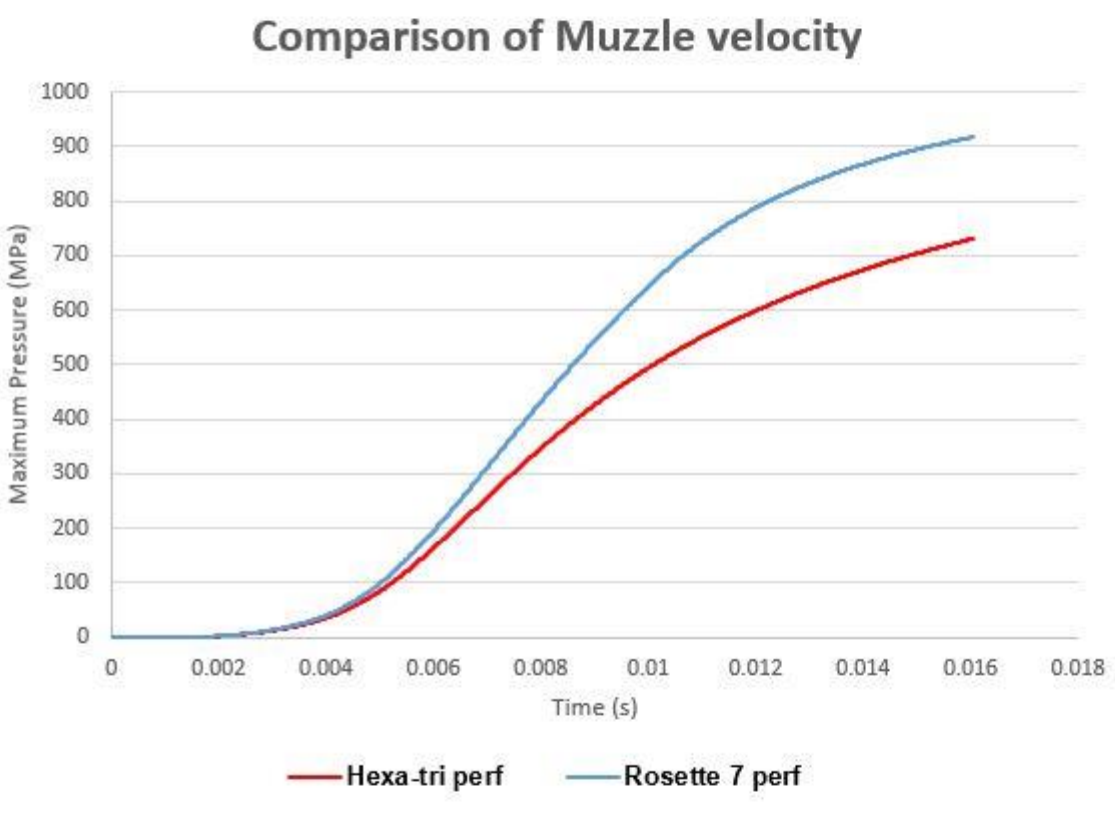

5.4 Web optimization

The web optimization stage is extremely vital during the development of new design propellant grain. basically, web optimisation is to vary the web thickness of the propellant grain and observe its effects on the outputs of the IB simulation model. The optimum web thickness is that the web thickness that gives the highest muzzle velocity with lowest chamber pressure. However, the charge mass is also very important as the 155mm artillery system is limited with chamber volume.

Because of the limitations of chamber size the maximum charge mass cannot be more than the determined value. As the perfect mass is lower than 13522 grams the highest MV with this charge mass can now be determined.. Then the charge mass will be manipulated until it matches the reference charge mass, which will be used to compare the predicted muzzle velocity with the proposed propellant.

5.4.1 Hexa tri-perf web optimisation analysis

The following figure shows the web optimisation analysis which carried out on the proposed propellant grain. the following is the procedure followed throughout the analysis:

1. The target muzzle velocity is fixed, which is to be 918 m/s.
2. The web thickness is determined by the outer radius of the propellant grain.
3. At each simulation run, the charge mass of the propellant is adjusted to achieve the fixed muzzle velocity of the 155mm artillery system, which is 918 m/s.

The following figure shows the required propellant mass at certain web thickness to achieve the required muzzle velocity and maximum chamber pressure.

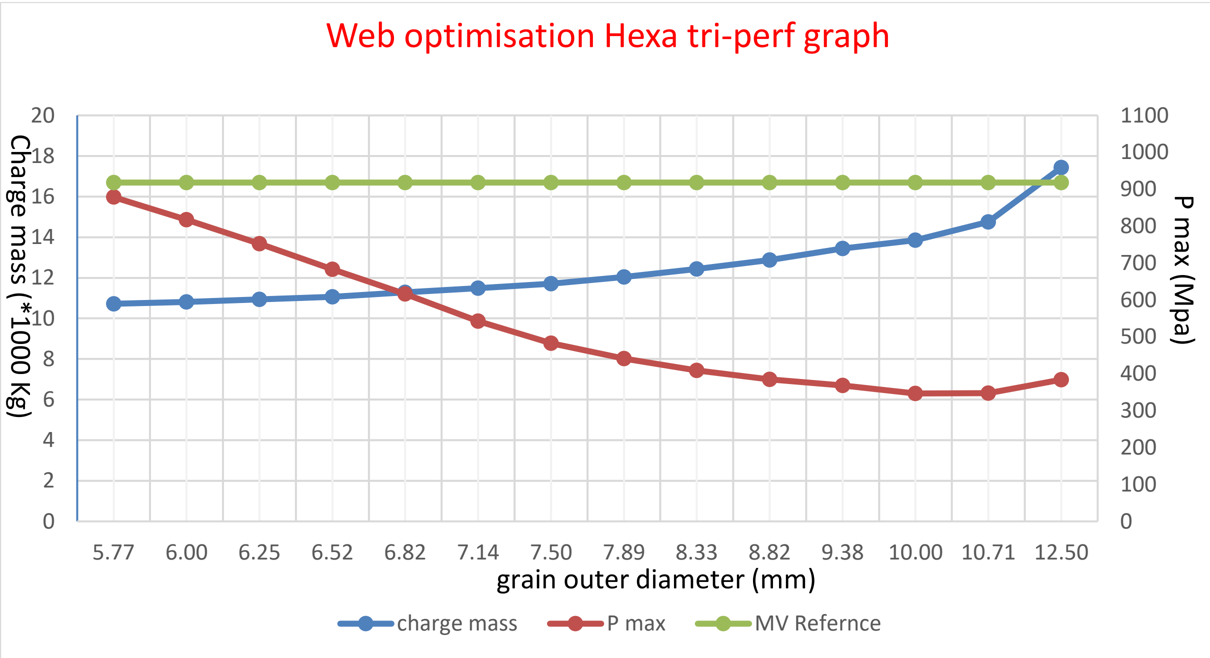

Figure 46: Web optimisation Hexa tri-perf graph

The table below represents the output of the web optimisation analysis. The criteria of the optimum web selection are that the selected web shall give the lowest maximum pressure value, the highest muzzle velocity, and the required charge mass. The highlighted column of the following table is the selected web thickness to carries out the rest of the analysis. After selecting the optimum web, the comparison between the proposed propellant grain as well as the rosette grain can take place.

Table 10: Hexa tri-perf web optimisation

Grain outer diameter (mm)	charge mass (kg)	P max (MPa)
12.50	17.43	383.46
11.54	15.96	360.03
10.71	14.75	347.11
10.00	13.85	346.59
9.38	13.44	368.48
8.82	12.88	384.60
8.33	12.43	409.39
7.89	12.05	441.22
7.50	11.71	482.82
7.14	11.48	542.50
6.82	11.29	616.34
6.52	11.07	682.69
6.25	10.93	752.50
6.00	10.82	817.57
5.77	10.72	878.53

5.5 Discussion of results

Table 11 summarises the results of the internal ballistics simulation of 155mm artillery system using the optimised newly developed propellant grain as well as the rosette grain.

Table 11: Internal ballistic properties before and after web optimisation

Grain properties		After Web optimisation	
Shape	Mass (g)	Maximum P (MPa)	MV (m/s)
rosette (Reference)	13522	333	918
hexa tri-perf	13440	368.48	918
Deviation	82	35.48	0

As can be seen, the charge mass almost the similar between the rosette and the developed propellant grain. Furthermore, the muzzle velocity is also similar between the developed and the rosette grain. However, the maximum chamber pressure of the rosette is less than the developed propellant grain. The difference between both grain is 35 MPa, which is classified as a relatively large.

The figure below shows the comparison between the burning surface area versus burnt fraction.

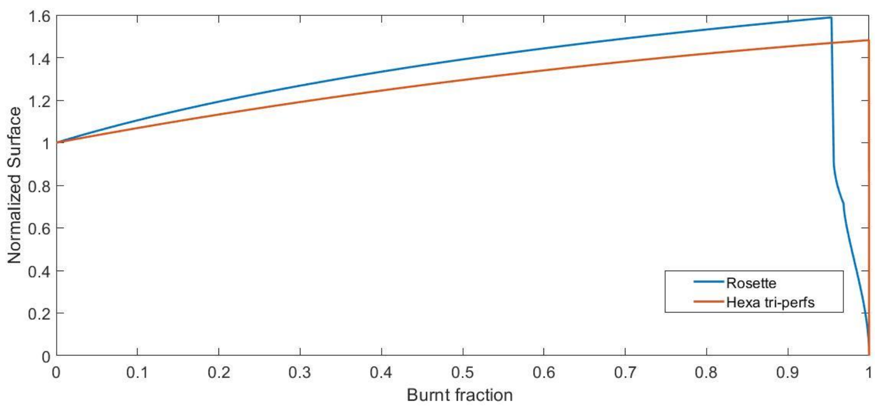

Figure 47: comparison between the burning surface area versus burnt fraction

5.6 Packing density

In the manufacturing process, the nesting software is used when cutting metal sheets using a laser cutter to achieve high accuracy and minimise unused areas in the sheets (wastage). This research benefits from this process if the sheet is the charge, and the cutting tool is the propellant shape. By this analogy, the software will replicate the packing. The nesting process is a complicated mathematical exercise. It provides 10 possible stacking options through an optimisation process where the shape is turned 0, 10, 15, 30, 45, 90 and 180 degrees to utilise as much space possible within the charge. Thereafter the software prints a report that illustrates the packing process that occurred its results and the efficiency of the nesting used. The results can be used to calculate the packing efficiency through the following formula.

$$\text{Packing efficiency} = \frac{Area\ grain}{Area\ charges} * 100$$

Equation 3-2

5.6.1 Packing density verification

In this section using two software programs TruNest and MyNesting the required test has been performed. The tests will be performed on the two grain geometries hexa tri-perf and rosette. The following results were obtained and verified by comparing the two software outcomes as shown in Table 12.

Table 12: Packing efficiency result for rosette and hexa tri-perf

			Packing efficiency	
Grain shape	**area of charge case**	**occupied area by the grains**	**MyNesting**	**TruNest**
Rosette	0.01738	0.01353	77.8%	78.0%
hexa tri-perf	0.01738	0.01397	80.4%	80.4%

From the TruNest results, there are several conclusions which can be drawn. The packing efficiencies of the rosette and hexa tri-perf grains are 78% and 80% respectively. According to these results there is a difference between rosette nesting and hexa tri-perf nesting of around 2.38%, so the hexa tri-perf have a higher packing efficiency than the rosette grain. The two packing techniques achieve the same results for very different grain shapes consider to be verified. This finding is very important when determining the efficiency of the packaging process.

In this research, our goal is to design a technique that will be used to utilise space using packing density analysis. As it has been established through a literature review, it is very important to consider the space usage in the charge for propellants to attain the required propulsion. The more stacked the propellants are in the propellant charger, the higher the degree of propulsion attained. The difference between modern technology and earlier technology is efficiency and safety during firing. Guns used in the past were very large in volume but could not achieve much as these volumes were not adequately utilised. To overcome this problem, guns developed today have small volumes and better performance. This performance is obtained from effective space utilisation and better packing densities. The application of computational geometry to the packing problem has produced more efficient guns.

In this study, a comparison was made between two grain shapes of propellant to find the highest packing density to obtain the highest level of performance. In the analysis, two grain shapes, hexa tri-perf and rosette, were evaluated. This analysis was done using two software applications (TruNest and MyNesting). The results that were obtained in this analysis are shown in Table 14.

It is very important to remember that the main goal of this research is to determine the criteria that can be applied to ensure that there is increased packing density in the propellant charger. Since the tests made have similar results between the two packing techniques, it is concluded that the two approaches are similar. To differentiate them it was determined that hexa tri-perf are known to resolve industrial packing problems compared to rosette grains with 2.38% greater packing efficiency. For this reason, it is recommended that the best grain shape that could be used to achieve the objective is hexa tri-perf.

5.7 Conclusions

In this chapter, the 155mm artillery system is simulated via the IB simulation model utilising rosette grain and the newly developed propellant grain. The results of the simulation were compared. After the comparison, the developed propellant grain underwent web optimisation analysis. Then, the optimum web thickness was selected, which gives the least chamber pressure and highest muzzle velocity. The optimised propellant grain was compared to the rosette grain in term of performance using the interior ballistic simulation model. Finally, the optimised propellant grain was compared to the rosette grain in term of the packing density.

Chapter 6 - CONCLUSIONS and RECOMMENDATIONS

6.1 Research overview

In Chapter 1, the research aims to design a new propellant grain geometry that, when to combust it produce minimum slivers, thus improving the efficiency of a large caliber system. This research also provides a proposed propellant grain geometry that has a higher packing density while retaining good propellant ignition.

In Chapter 3, the tool used to obtain the expected results of the internal ballistic process is introduced. This research has required the development of an internal ballistic code proposed by the STANAG specification; it has been developed in MATLAB to calculate muzzle velocity, pressure and propellant mass in the IB cycle.

In Chapter 4, a method was found to verify the form function used in the code that calculates the surface area of the propellant; this is done by comparing the surface area, which is a result of the form function, and equating it with the surface area resulting from the Solid Edge software, which measures the surface area of complex geometric shapes.

in Chapter 5 a mass determination process was performed to identify the amount of propellant needed to achieve the specified muzzle velocity. The web optimization was carried out, which produced the results required for a comparison with the rosette grain.

6.2 The Method of Investigation

The method of investigation of this study was:

1. Propose a new shape for the propellant.
2. Propose a method that ensures the minimising of slivers by an offset tool available in the Solid Edge software.
3. Present a form function for the proposed propellant that calculates all the variations in the surface area and the size of the grain propellant.
4. Verify the surface area and size results from the form function and compare them to the results of the surface from the solid edge.
5. Provide a code that calculates the expected results for the muzzle velocity and maximum pressure for the 155 mm system.
6. Provide a procedure to determine the optimum mass required by using web optimisation of the propellant grains.

7. Compare of the proposed propellant with the rosette grain used by RDM through the results of the internal ballistics and packing density.

6.3 Conclusion

The aim of this research was to develop new propellant grain that has a better performance than the rosette grain in term of sliver formation. In addition to that, the newly developed propellant grain must achieve higher packing density than the rosette grain. This research proposed new propellant grain that might has a better performance than the rosette grain in term of the sliver formation as well as the packing density.

However, after all the analysis, the developed propellant grain seems that there is a possibility of sliver formation. In addition to that, the rosette grain has a better performance in term of the maximum chamber pressure. However, the developed propellant grain achieves higher packing density than the rosette grain. The newly developed propellant grain might not be a better alternative to the rosette grain. However, it might just be a beginning of discovering better alternative to the rosette grain. In addition to that, this research formulates a framework that to be used to develop new propellant grain.

6.4 Future work

Although the proposed design seems to be unpromising design, the framework that developed throughout this research to develop new propellant grain seems to be promising. Therefore, the framework can be improved, verified, and validated as it might give robust framework to be considered when developing new propellant design.

Slivering of this design is another area to be considered in future work. It is to take the newly developed propellant grain under further investigation in term of slivering and if the result is promising then the grain can be validated.

References

AÇIK, S. (2010). Internal ballistic design optimization of a solid rocket motor. *Middle East Technical University*, 38-39.

Anderson, R. D. (1987). *IBHVG2 A USER'S GUIDE.* MARYLAND: US ARMY BALLISTIC RESEARCH LABORATORY.

Army Materiel Command, U. S. (1965). *Internal Ballistic of Guns.* U.S. Government Printing Office. Retrieved from https://books.google.co.uk/books?id=zmZUf_h-ak0C

Atwood, A. I., Boggs, T. L., Curran, P. O., Parr, T. P., Hanson-Parr, D. M., Price, C. F., & Wiknich, J. (1999). SOLID PROPELLANT FLAME STRUCTURE - Burning Rate of Solid Propellant Ingredients, Part 1: Pressure and Initial Temperature Effects. *Journal of propulsion and power. 15, no. 6, (1999): 740*.

Brooks, W. T. (1972). *Solid propellant grain design and internal ballistics (Vol. 8076).* [Washington] : National Aeronautics and Space Administration : [For sale by the National Technical Information Service, Springfield, Va.].

Canada, G. D. (2019, 03 04). *Military and Commercial Energetic*. Retrieved from General Dynamics Canada: https://www.gd-otscanada.com/product/energetic-materials/

Carlucci, D. E., & Jacobson, S. S. (2018, 12 12). *Ballistics : Theory and Design of Guns and Ammunition, Third Edition.* Boca Raton, FL : CRC Press, 2018. Retrieved from E-ballistics Fundamentals of Ballistics: https://e-ballistics.com/ebook/internal%20ballistics%20-%20energy%20balance.htm#Friction

Carlucci, D. J. (2007). *BALLISTICS THEORY AND DESIGN OF GUNS AND AMMUNITION.* London: Taylor & Francis Group, LLC.

Chaturvedi, S., & Dave, P. N. (2015). Solid propellants: AP/HTPB composite propellants. *Arabian Journal of Chemistry, (201501)*.

Chaturvedi, S., & Dave, P. N. (n.d.). Solid propellants: AP/HTPB composite propellants. *Arabian Journal of Chemistry, (201501)*, 2015.

Command., U. S. (2019, 02 10). *Engineering design handbook : ballistics series : interior ballistics of guns, 1965.* (Vols. AMC pamphlet, 706-150.). [Washington] : [U.S. G.P.O.], [1965]. Retrieved from fas.org.

Dyckmans, G. (2015, 12 1). *Fundamentals of Ballistics*. Retrieved from E-ballistics: https://e-ballistics.com/ebook/internal%20ballistics%20-%20energy%20balance.htm#Friction

Dyckmans, G. (2018, 12 11). *Fundamentals of Ballistics: Internal Ballistics*. Retrieved from E-ballistics: https://e-ballistics.com/ebook/internal%20ballistics.htm

E.C. Hansen, O. H. (1987). *PRESSURE AND GAS FLOW GRADIENTS BEHIND THE PROJECTILE DURING THE INTERIOR BALLISTIC CYCLE.* Florida : University of Florida.

FUNDA YILDIRIM, E. T. (2012). OPTIMAL PROPELLANT GRAIN GEOMETRY DESIGN FOR LARGE. *International Scientific Conference on Defensive Technologies, Belgrade*, 217.

George, S., & Oscar, B. (2001). *Rocket Propulsion Elements* (Seventh Edition ed.). A Wiley-Interscience publication.

Hafner, M. T. (2014). *U.S. Patent No. Patent No. 8,641,842. Washington, DC: U.S. Patent and Trademark Office.*

Hall, N. (2018, 12 12). *Conservation of Energy*. Retrieved from NASA: https://www.grc.nasa.gov/www/k-12/airplane/thermo1f.html

Johnston, I. A. (2005). *The Noble-Abel Equation of State: Thermodynamic Derivations for Ballistics Modelling.* AUSTRALIA: DEFENCE SCIENCE AND TECHNOLOGY ORGANISATION EDINBURGH (AUSTRALIA) WEAPONS SYSTEMS DIV.

Johnston, I. A. (2005). *The Noble-Abel Equation of State: Thermodynamic Derivations for Ballistics Modelling.* Edinburgh: Defence Science and Technology Organisation.

Kent, J. A. (2003). *Riegel's Handbook of Industrial Chemistry.* Springer, Boston, MA: New York, NY : Springer US : Imprint : Springer, .

Khaikov, V. (2018). SOLID PROPELLANT FLAME STRUCTURE - Burning Rate of Solid Propellant Ingredients, Part 1: Pressure and Initial Temperature Effects. *Vojnotehnicki glasnik, v66 n2 (2018): 281-303*.

Kubota, N. (2007). *Propellants and Explosives Thermochemical Aspects of Combustion.* Weinheim: WILEY-VCH Verlag GmbH & Co. KGaA.

Li, K., & Zhang, X. (2011). Multi-Objective Optimization of Interior Ballistic Performance Using NSGA-II. *Propellants, Explosives, Pyrotechnics, v36 n3 :*, 282-290.

Luděk Jedlicka, S. B. (2007). PRESSURE DISTRIBUTION IN THE SPACE BEHIND A PROJECTILE . *Advances in MT*, 35-48.

Meyer, R., Köhler, J., Homburg, A., & KGaA., W.-V. V. (5 November 2007). *Explosives 6th.* Wiley-VCH Verlag GmbH, Weinheim, 2007.

Miner, R. (2013). Computational interior ballistics modeling.

Minor, C. R. (1985). *MULTIZONE MODULAR ARTILLERY PROPELLING.* MARYLAND: US ARMY BALLISTIC RESEARCH LABORATORY.

Moreno, J. A. (2009). *Thermodynamic Interior Ballistic Model With Global Parameters.* NATO Standardization Agency.

Morrison, W. F., Wren, G. P., Oberle, W. F., & Richardson, S. L. (1993). *The Application of Lagrange and Pidduck-Kent Gradient Models to Guns Using Low Molecular Weight Gases.* Ft. Belvoir Defense Technical Information Center.

National Aeronautics, A. U. (1972). Solid Propellant Grain Design and Internal Ballistics. NASA SP-8076. *NASA SP-8076, 98 pages, published by NASA, Washington, D.C.*

NATO. (2000). *Thermodynamic Interior Ballistic Model with Global Parameters 2nd ed.* Brussels: MAS and BMS.

NATO. (2009). *Thermodynamic Interior Ballistic Model With Global Parameters.* NATO Standardization Agency.

Pandey, K. C. (2013). Burnback Analysis of 3-D Star Grain Solid Propellant. *International Journal of Advanced Trends in Computer Science and Engineering, Vol.2 , No.1,*, Pages : 215-223.

Pearson, D. S. (1987). *Recent Advances in the Molecular Aspects of Polymer Viscoelasticity.* New Jersey: Exxon Research and Engineering Company, Route 22 East, Annandale, New Jersey 08801.

RDM, R. D. (2016). *internal ballisticians.* Somerset West.

RDM, R. D. (2018). *RDM Internal Ballistic.* somerset west.

Roman Wölbing, M. C. (2018). Numerical Simulations of Reactive Two-Phase Flows in Interior. *Proceedings of the 3rd World Congress on Momentum, Heat and Mass Transfer (MHMT'18)*, CSP 113-1 CSP 113-5.

Russell, M. S. (2009). *The Chemistry of Fireworks.* Cambridge: The Royal Society of Chemistry.

Ruth, C. R., Minor, T. C., & MD., A. B. (1985). *Multizone Modular Artillery Propelling Charge Studies* (Vols. CAI-LCA-CM9700151-REV 0). Ft. Belvoir Defense Technical Information Center FEB .

S., J. S. (1977). *The United States of America Patent No. US4094248A.*

Scepaniak, A. (2014, 11 13). *Polygonal Rifling in Glocks: Why It Matters!* Retrieved from theguns and gear store: https://blog.thegunsandgearstore.com/polygonal-rifling-in-glocks-why-it-matters/

Schabort, V. (2016). *RDM Internal Ballistic.* Somerset West: RDM.

Shekhar, H. (2015). *Effects of the Burning Rate Index on the Pressure Time Profile of Progressive Burning Tubular Rocket Propellant Configurations.* Central European Journal of Energetic Materials, v12 n2 (20150101).

Speck, P. L. (1995). *United States Patent No. US5821449A.*

STANAG 4367, A. N. (2012). STANAG 4367 (EDITION 3) - THERMODYNAMIC INTERIOR BALLISTIC MODEL WITH GLOBAL PARAMETERS. 1-42.

Tola, C., & Nikbay, M. (2018). Solid Rocket Motor Propellant Optimization with Coupled Internal Ballistic—Structural Interaction Approach. *Journal of spacecraft and rockets, 55, no. 4, (2018): 936-947*, 1-13.

W. F. Morrison, G. P. (1993). *The Application of Lagrange and Pidduck-Kent Gradient Models to Guns Using Low Molecular Weight Gases.* U.S. Army Research Laboratory.

W., F., & Vanderhoff, J. A. (May 1993). *A Summary of the JANNAF Workshop on Methods for Exchange of Gun Propellant Burning Rate Information.* U.S: Aberdeen Proving Ground, Md. : U.S. Army Research Laboratory.

Warren, R. C., & Starks, A. T. (1988). *Multiple Flow Regimes in the Extrusion of Nitrocellulose Based Propellant Doughs.* AUSTRALIA: WEAPONS SYSTEMS RESEARCH LAB ADELAIDE.

White, K. J. (1997). *Effect of propellant grain dimensions on progressivity .* Ft. Belvoir Defense Technical Information Center OCT 1997.

White, K. J., Oberle, W. F., Juhasz, A. A., Stobie, I. C., & Nekula, K. (1995). *Electrothermal-Chemical (ETC) Propulsion with High Loading Density Charges.* (No. ARL-TR-845). ARMY RESEARCH LAB ABERDEEN PROVING GROUND MD.

Xiao, Z. Y. (2015). Interior ballistic prediction of gun propellants based on experimental pressure-apparent burning rate model in closed vessel. *Science and Technology of Energetic Materials*, Vol. 76, pp. 1–7.

Yang, V., Brill, T. B., & Ren, W.-Z. (2000). *Solid propellant chemistry, combustion, and motor interior ballistics. American Institute of Aeronautics and Astronautics.* Reston, Va. : American Institute of Aeronautics and Astronautics,.

Zeller, B. (1993). *Solid propellant grain design. In Solid rocket propulsion technology (pp. 35-84). Pergamon.* Pergamon Press.